Geological Magazine

www.cambridge.org/geo

Original Article

Cite this article: Liu S, Feng C, Feng G, Fan Y, and Guo Z (2023) Early Precambrian mafic dykes in western Shandong province, North China Craton: constraints on the chronology, genetic model and tectonic significance. *Geological Magazine* **160**: 1041–1064. https://doi.org/10.1017/S0016756822000784

Received: 18 October 2021
Revised: 3 July 2022
Accepted: 6 July 2022
First published online: 2 May 2023

Keywords:
Neoarchaean; mafic dykes; zircon geochronology; geochemical modelling; NCC

Author for correspondence:
Shen Liu,
Email: liushen@nwu.edu.cn

Early Precambrian mafic dykes in western Shandong province, North China Craton: constraints on the chronology, genetic model and tectonic significance

Shen Liu[1], Caixia Feng[1], Guangying Feng[2], Yan Fan[1] and Zhuang Guo[1]

[1]State Key Laboratory of Continental Dynamics and Department of Geology, Northwest University, Xi'an 710069, China and [2]Institute of Geology, Chinese Academy of Geological Sciences, Beijing 100037, China

Abstract

In the Late Neoarchaean, the lithosphere of the North China Craton (NCC) experienced a strong extensional event, which is of great significance for understanding the evolution of the continental crust in the Precambrian. In this study, a suite of mafic dykes from Shandong province in the northeastern NCC were investigated to determine the nature, timing and source of rift-related magma activities using zircon U–Pb data, whole-rock geochemistry and Nd–Hf isotopes. Zircon U–Pb dating of four dolerites by laser ablation – inductively coupled plasma – mass spectrometry (LA-ICP-MS) yielded weighted mean $^{207}Pb/^{206}Pb$ ages in the range 2509 ± 6.1 to 2537 ± 6.2 Ma (2σ, 95 % confidence interval). The mafic dykes are classified as alkaline rocks based on their $K_2O + Na_2O$ contents (6.78–7.21 wt %) and belong to the shoshonitic series according to their K_2O contents (3.23–3.36 wt %). The dolerites show low concentrations of light rare earth elements ($(La/Yb)_N$ between 7.17 and 8.55), positive Eu anomalies (Eu/Eu* between 1.12 and 1.27), positive Ba, K, Pb, Sr, Eu, Dy and Lu anomalies, and depleted U, Nb, Pr, Ta, P, Nd and Ti anomalies. The dykes are characterized by low initial $(^{87}Sr/^{86}Sr)_i$ (~0.6969), positive $\varepsilon_{Nd}(t)$ values (0.2–0.8) and $\varepsilon_{Hf}(t)$ values (0.5–8.6) and relatively old mean Nd and Hf model age (2.73 Ga). Collectively, the data suggest that the mafic dykes were derived from the partial melting (10–20 %) of an isotope-depleted garnet–lherzolite mantle source that was hybridized through interaction with subducted lower crustal material. The parental magmas of these dykes underwent a certain number of crustal contaminations during magma ascent. The mafic magmatism represented in the form of the dyke swarms is considered to be a response to widespread lithospheric extension which affected the NCC at *c.* 2.5 Ga during the Neoarchaean.

1. Introduction

The North China Craton (NCC) was formed by welding several Archaean micro-continents along a marine closed greenstone belt (Zhai & Santosh, 2011; Yang *et al.* 2016; Tang & Santosh, 2017; Yang & Santosh, 2017). A large number of ~2.5 Ga rock units were preserved in the NCC (Wu *et al.* 1998; Zhai & Bian, 2000; Zhai, 2010). The NCC covers a vast area of eastern China (Wu *et al.* 2008), which includes two ancient continental cores of *c.* 3.8 Ga age (Jahn & Bai, 1983; Huang *et al.* 1986; Liu, 1991; Liu *et al.* 1992, 1994; Song *et al.* 1996; LQ Wang *et al.* 1998; Zheng *et al.* 2004; Gao *et al.* 2005; Shen *et al.* 2005; Wan *et al.* 2005; Geng *et al.* 2007; HL Wang *et al.* 2007; Diwu *et al.* 2008; Chen *et al.* 2009; Zhang *et al.* 2009). The NCC was finally cratonized in the Late Palaeoproterozoic, thus recording a complex Precambrian evolution history. All crustal fragments gathered in the unified NCC were merged into the Columbia supercontinent (Santosh, 2010; Zhao & Zhai, 2013). In addition, the NCC underwent an extensional regime between 2.5 and 2.45 Ga (Zhai & Peng, 2007), leading to basement uplift, formation of rift-related troughs, and major anorogenic magmatism represented by the emplacement of granitoid suites (e.g. Song *et al.* 1996) and mafic dykes. The events related to the emplacement of the mafic dykes can provide important information about the formation and evolution of the early crust. To date, more than 100 Proterozoic (<2.5 Ga) mafic dykes have been found in the NCC including those in the Hebei, Shanxi and Shandong area with ages ranging from 800 to 600 Ma, 820 Ma, 900 Ma, 925 Ma, 1.78 Ga and 2.4 to 1.6 Ga. They have been widely studied (Li *et al.* 1997; Zhai & Bian, 2000; Peng *et al.* 2005, 2007, 2008, 2010, 2011*a*, *b*; Hou *et al.* 2006; Peng, 2010; Hou, 2012; Li, 2014). Nevertheless, only a few investigations of the Archaean mafic dykes (>2.5 Ga) have been carried out in the NCC.

At present, the western part of Shandong province has been the focus of several studies related to the Early Precambrian evolutionary history of the NCC (Hou, 2012). Approximately 95 % of the Early Precambrian crystalline basement in western Shandong is

© The Author(s), 2023. Published by Cambridge University Press.

dominated by granulites, greenstones, Trondhjemite-Tonalite-Granodiorite (TTG) gneisses, gneissic monzogranite, dioritic to granodioritic intrusions, and mafic dyke swarms (Wang, 1990; Hou *et al.* 2004; Ju *et al.* 2014). In addition, the TTG series rocks and gneissic monzogranites in this area have been divided into two stages (2.5–2.6 Ga, 2.45–2.56 Ga; Jahn, 1988; Wang, 1991, 1993). The mafic dykes in western Shandong province are generally NE–SW-trending and are mainly located in the Tai'an, Laiwu and Mengyin regions (Hou, 2012).

Herein, we present new zircon $^{207}Pb/^{206}Pb$ ages, and petrological, whole-rock geochemical and Nd–Hf isotopic data on the mafic dykes studied from western Shandong province, northeastern NCC. Our results constrain the emplacement ages and the origin of the dykes and provide insights into the tectonic significance of the NCC during the Neoarchaean.

2. Geological setting and petrography

As a part of the Sino-Korean Craton, the Precambrian crustal evolution history of the NCC and the extensive Mesozoic redemption events have attracted global attention (Griffin, 1992; Griffin *et al.* 1998; O'Reilly *et al.* 2001; Xu, 2001; Zhang *et al.* 2003; Zhai & Santosh, 2011, 2013; Zhao & Zhai, 2013; Deng *et al.* 2017; Li & Santosh, 2017). The NCC is bounded by the Early Palaeozoic Qilianshan Orogen to the west, the Late Palaeozoic Tianshan – Inner Mongolia – Daxinganling Orogen of the Central Asian Orogenic Belt to the north and the Mesozoic Qinling–Dabie–Sulu high/ultrahigh-pressure metamorphic belt to the south (Zhao, 2013).

According to the structural subdivision view of the NCC, it is composed of two north–south-trending Palaeoproterozoic (1.85 Ga) eastern and western crustal blocks welded across the North China Orogenic Belt (Zhao *et al.* 2001, 2005; Wilde *et al.* 2002; Guo *et al.* 2005). The Eastern Block experienced obvious lithospheric thinning in the Late Mesozoic, and it contains many world-class gold deposits (Goldfarb & Santosh, 2014; Li & Santosh, 2017). It separates the Longgang Block from the Langlin Block and retains the oldest continental crust of the NCC (Fig. 1; Li *et al.* 2006, 2012; Li & Zhao, 2007; Luo *et al.* 2008; Zhou *et al.* 2008; Tam *et al.* 2011, 2012*a*, *b*, *c*; Dan *et al.* 2012, 2014; Zhang *et al.* 2013). The Western Block has thick lithospheric roots across Shanxi, Shaanxi, Inner Mongolia and Northern Gansu provinces. It has become the most stable part of the NCC (Santosh, 2010). It is a collage of the Northern Yinshan and Southern Ordos Blocks along the Inner Mongolia Suture Zone, merging the Palaeoproterozoic Khondalite Belt (Fig. 1; Xia *et al.* 2008; Yin *et al.* 2009, 2011; Santosh, 2010; Li *et al.* 2011; Wang *et al.* 2011; Dan *et al.* 2012, 2014; Zhang *et al.* 2013; Yang *et al.* 2016). The southern and northern edges of the NCC are marked by the Indosinian Qinling Dabie and Hercynian Yinshan Yanshan Orogenic Belts. Its western edge borders Helan Qilian Orogenic Belt, and its eastern edge is located in Korea. The NCC is composed of uniform Precambrian crystalline basement, which is covered by younger overburden (Zhao *et al.* 2001) and invaded by the Precambrian and Mesozoic mafic dyke swarms (e.g. Li *et al.* 1997; Zhai and Bian, 2000; Hou *et al.* 2004, 2006; Liu *et al.* 2004, 2005, 2008*a*, *b*, 2009, 2012*a*, *b*, 2013*b*; Peng *et al.* 2005, 2007, 2008, 2010, 2011*a*, *b*; Peng, 2010; Hou, 2012). Another model suggests that the NCC is composed of several Archaean micro-continental blocks and these blocks have been proliferated into large continental fragments (Zhai & Bian, 2000; Zhao, 2009; Zhai & Santosh, 2011; Dan *et al.* 2012, 2014; Zhang *et al.* 2013; Yang *et al.* 2016; Yang & Santosh, 2017).

The fresh near-vertical mafic dykes in the study area are NE–SW-trending and intruded into luxiwu well in northeast North Carolina. The Early and Middle Proterozoic strata in the Mawangyu and Zhujiayu areas (Tables 1–5) have dykes extending from 3.0 to 9.0 km and a width range of 25–1.0 m. The rock types include gabbro, dolerite and diabase porphyry. Wujing dykes phenocrysts (WJA1–8, WJB1–8) include medium-grained clinopyroxene (2.5–6.5 mm) and tabular plagioclase (2.0–5.5 mm), and the matrix is composed of clinopyroxene (0.04–0.05 mm), plagioclase (0.03–0.06 mm), a small amount of magnetite (0.02–0.03 mm), secondary chlorite (0.03–0.05 mm) and auxiliary zircon composition (Fig. 1). The dyke phenocrysts of Mawangyu and Zhujiayu (MWY1–7, ZJY1–7) include medium-sized clinopyroxene (2.5–5.0 mm) and tabular plagioclase (2.0–5.0 mm), and the matrix consists of clinopyroxene (0.04–0.06 mm), plagioclase (0.03–0.05 mm), secondary magnetite with auxiliary zircon and apatite (0.02–0.03 mm) and secondary chlorite (0.04–0.06 mm) (Figs 1, 2).

3. Sampling and analytical techniques

Thirty samples were collected from the mafic dykes (Fig. 1). Zircon grains were separated from four samples (WJA1, WJB3, MWY2 and ZJY1) using conventional heavy liquid and magnetic techniques at the Langfang Regional Geological Survey, Hebei province, China. After separation and mounting, the morphology and internal structure of the zircons were imaged using transmitted and reflected light and by cathodoluminescence (CL) techniques at the State Key Laboratory of Continental Dynamics (SKLCD), Northwest University, Xi'an (Fig. 3). Prior to zircon U–Pb dating, grain mount surfaces were washed in dilute HNO_3 and pure alcohol to remove any potential lead contamination. Zircon U–Pb and $^{207}Pb/^{206}Pb$ weighted average ages were determined by LA-ICP-MS (Table 1; Fig. 4) using an Agilent 7500a ICP-MS instrument equipped with a 193 nm excimer laser at the SKLCD. The zircon standard 91500 was used for quality control, and a NIST 610 standard was used for data optimization. A spot diameter of 24 μm was used during analysis, employing the methodologies described by Liu *et al.* (2010*a*). Common Pb correction was undertaken following the approach of Andersen (2002), and the resulting data were processed using GLITTER and ISOPLOT (Ludwig, 2003; Table 1; Fig. 4). Uncertainties on individual LA-ICP-MS analyses are quoted at the 95 % (1σ) confidence level.

In situ zircon Hf isotope analysis was performed on Nu plasma Human Resource (HR) MC-ICP-MS equipped with a geolas 2005 193 nm ArF excimer laser ablation system. Analyses were carried out using a spot size of 44 μm, and He was used as the carrier gas. The laser repetition rate is 10 Hz and the energy density applied is between 15 and 20 J cm^{-2}. During the analysis, the $^{176}Hf/^{177}Hf$ ratio of the standard zircon (91500) was 0.282295 ± 0.000027 ($n = 14$; 2σ), which is in good agreement with the recommended $^{176}Hf/^{177}Hf$ ratios within 2σ (0.282308 ± 58, 2σ; 0.282015 ± 0.000029, 2σ) (Griffin *et al.* 2006; Wu *et al.* 2006). All the above analysis was performed at the SKLCD.

Whole-rock chemistry was completed at the State Key Laboratory of Deposit Geochemistry (SKLDG, Xi'an, Shaanxi Province), Institute of Geochemistry, Chinese Academy of Sciences. Using a molten glass disc, the analytical accuracy was better than 5 % according to Chinese national standard GSR-3 (Table 2). Loss on ignition was obtained using 1 g powder heated

https://doi.org/10.1017/S0016756822000784 Published online by Cambridge University Press

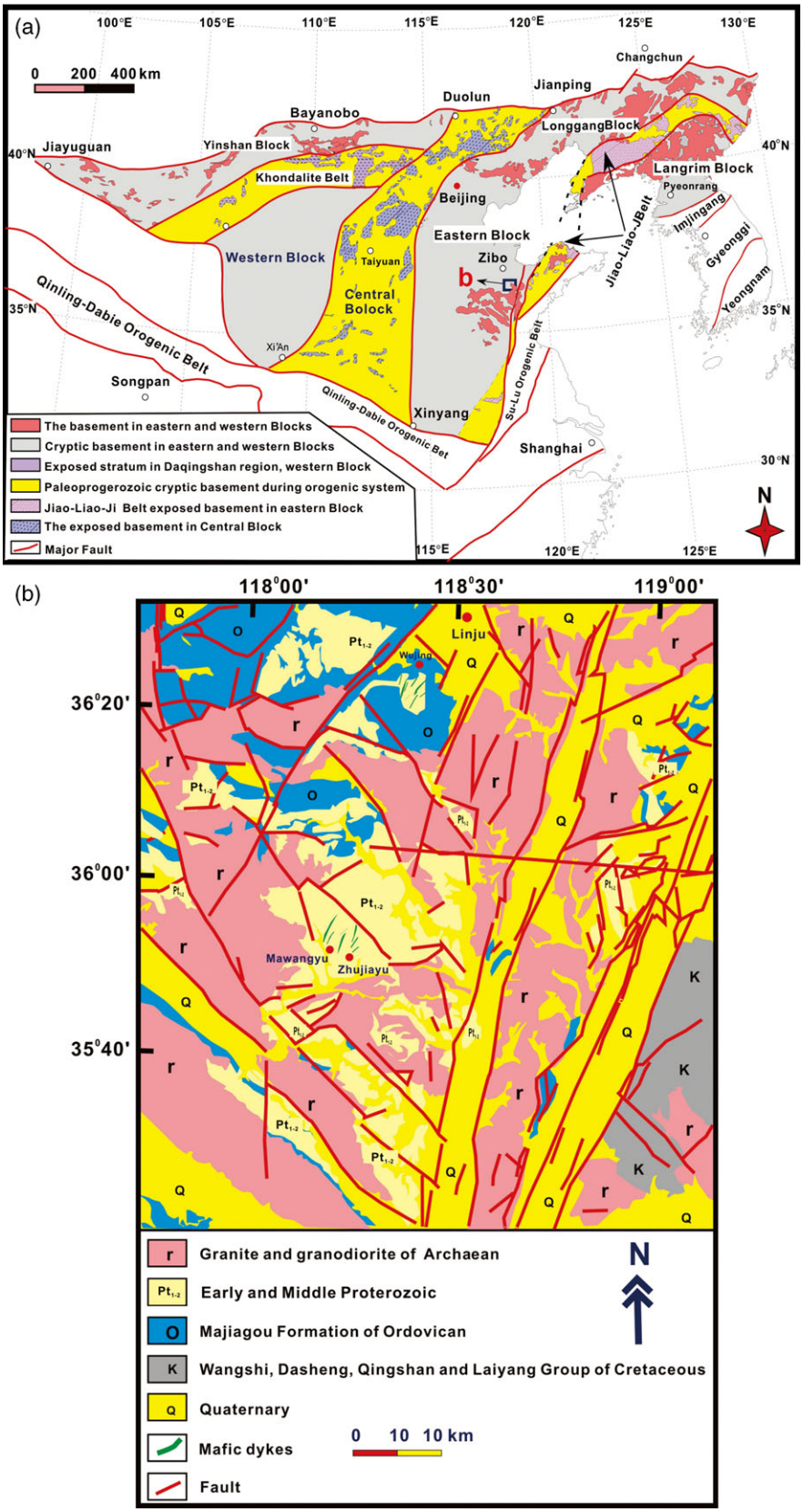

Fig. 1. (Colour online) (a) Location of the study area within the northeastern NCC. (b) Geological map of the study area, showing the distribution of mafic dykes studied and the location of samples collected during this study.

https://doi.org/10.1017/S0016756822000784 Published online by Cambridge University Press

Table 1. Zircon LA-ICP-MS U–Pb isotope data for the mafic dykes studied within western Shandong province, northeastern NCC

WJA01						Isotopic	ratios					Age (Ma)					
Spot	Th	U	Pb	Th/U	$^{238}U/^{232}Th$	$^{207}Pb/^{206}Pb$	1σ	$^{207}Pb/^{235}U$	1σ	$^{206}Pb/^{238}U$	1σ	$^{207}Pb/^{206}Pb$	1σ	$^{207}Pb/^{235}U$	1σ	$^{206}Pb/^{238}U$	1σ
1	165	242	341	0.68	1.32	0.1672	0.0025	10.68	0.08	0.4612	0.0035	2530	6	2496	7	2445	15
2	82	108	120	0.76	1.31	0.1666	0.0026	10.86	0.09	0.4753	0.0036	2524	6	2511	8	2507	16
3	121	119	233	1.02	1.29	0.1671	0.0036	10.61	0.16	0.4606	0.0051	2529	12	2490	14	2442	23
4	142	213	297	0.67	1.32	0.1675	0.0031	10.39	0.12	0.4495	0.0038	2533	9	2470	11	2393	17
5	1111	1475	2210	0.75	1.34	0.1672	0.0028	10.67	0.11	0.4628	0.0038	2530	8	2495	10	2452	17
6	138	1615	276	0.09	1.28	0.1724	0.0008	3.276	0.038	0.1537	0.0012	2581	10	1475	9	922	7
7	201	273	390	0.74	1.33	0.1675	0.0026	10.72	0.11	0.4633	0.0039	2533	8	2499	10	2454	17
8	181	728	546	0.25	1.33	0.1668	0.0025	10.88	0.09	0.4739	0.0036	2526	6	2513	8	2501	16
9	110	101	186	1.09	1.31	0.1643	0.0026	10.62	0.09	0.4675	0.0036	2500	6	2490	8	2473	16
10	686	1342	985	0.51	1.26	0.1726	0.0006	1.656	0.008	0.0703	0.0003	2583	4	992	3	438	2
11	136	166	253	0.82	1.32	0.1676	0.0028	10.91	0.08	0.4716	0.0035	2534	6	2515	7	2491	15
12	86	109	158	0.79	1.31	0.1678	0.0025	10.96	0.1	0.4772	0.0039	2536	7	2520	8	2515	17
13	129	113	208	1.14	1.33	0.1666	0.0026	10.86	0.11	0.4729	0.0038	2524	8	2511	9	2496	17
14	146	195	261	0.75	1.32	0.1665	0.0025	10.95	0.1	0.4765	0.0038	2523	7	2519	8	2512	17
15	289	395	541	0.73	1.33	0.1668	0.0028	10.86	0.09	0.4713	0.0041	2526	7	2511	8	2489	18
16	89	226	241	0.39	1.31	0.1672	0.0027	10.93	0.13	0.4736	0.0042	2530	9	2517	11	2499	18
17	259	261	429	0.99	1.32	0.1665	0.0028	10.84	0.12	0.4738	0.0041	2523	9	2510	10	2500	18
18	102	137	191	0.75	1.33	0.1668	0.0027	10.85	0.11	0.4745	0.0039	2526	8	2510	9	2503	17
19	202	183	348	1.10	1.31	0.1669	0.0029	10.82	0.1	0.4696	0.0038	2527	7	2508	9	2482	17
20	124	122	217	1.01	1.32	0.1673	0.0026	10.23	0.09	0.4437	0.0036	2531	7	2456	8	2367	16
21	159	152	266	1.05	1.32	0.1673	0.0028	10.88	0.15	0.4762	0.0038	2531	13	2513	13	2511	17
22	106	110	182	0.96	1.34	0.1672	0.0026	10.96	0.12	0.4783	0.0046	2530	8	2520	10	2520	20
23	203	195	263	1.04	1.32	0.1673	0.0028	11.04	0.11	0.4784	0.0041	2531	7	2527	9	2520	18
24	128	136	231	0.94	1.33	0.1672	0.0026	10.98	0.16	0.4755	0.0053	2530	11	2521	14	2508	23
25	168	173	282	0.97	1.31	0.1645	0.0031	10.44	0.11	0.4589	0.0039	2502	8	2475	10	2435	17
WJB03						**Isotopic**	**ratios**					**Age (Ma)**					
Spot	Th	U	Pb	Th/U	$^{238}U/^{232}Th$	$^{207}Pb/^{206}Pb$	1σ	$^{207}Pb/^{235}U$	1σ	$^{206}Pb/^{238}U$	1σ	$^{207}Pb/^{206}Pb$	1σ	$^{207}Pb/^{235}U$	1σ	$^{206}Pb/^{238}U$	1σ
1	819	1186	1091	0.69	0.96	0.1666	0.0006	9.726	0.068	0.4232	0.0025	2524	5	2409	6	2275	11
2	690	901	1045	0.77	0.97	0.1663	0.0006	10.144	0.102	0.4423	0.0031	2521	8	2448	9	2361	14
3	995	1401	1331	0.71	0.95	0.1671	0.0007	10.766	0.097	0.4675	0.0032	2529	7	2503	8	2473	14
4	875	1103	955	0.79	0.96	0.1672	0.0008	10.933	0.122	0.4745	0.0036	2530	9	2517	10	2503	16
5	642	701	755	0.92	0.95	0.1671	0.0005	10.992	0.085	0.4786	0.0028	2529	6	2522	7	2521	12
6	714	805	719	0.89	0.95	0.1668	0.0008	7.172	0.091	0.3115	0.0026	2526	11	2133	11	1748	13
7	903	1246	1816	0.73	0.98	0.1668	0.0008	9.306	0.102	0.4045	0.0031	2526	9	2369	10	2190	14
8	603	529	1001	1.14	0.98	0.1672	0.0006	8.974	0.071	0.3895	0.0023	2530	6	2335	7	2121	11
9	756	899	823	0.84	0.97	0.1669	0.0007	8.493	0.085	0.3687	0.0026	2527	8	2285	9	2023	12
10	186	2612	692	0.07	0.96	0.1723	0.0005	3.295	0.018	0.1604	0.0008	2580	4	1480	4	959	4
11	768	824	903	0.93	0.95	0.1666	0.0007	10.694	0.126	0.4653	0.0036	2524	10	2497	11	2463	16
12	402	395	697	1.02	1.03	0.1665	0.0016	10.881	0.303	0.4742	0.0083	2523	25	2513	26	2502	36

(*Continued*)

https://doi.org/10.1017/S0016756822000784 Published online by Cambridge University Press

Table 1. (*Continued*)

WJB03						Isotopic	ratios					Age (Ma)					
Spot	Th	U	Pb	Th/U	$^{238}U/^{232}Th$	$^{207}Pb/^{206}Pb$	1σ	$^{207}Pb/^{235}U$	1σ	$^{206}Pb/^{238}U$	1σ	$^{207}Pb/^{206}Pb$	1σ	$^{207}Pb/^{235}U$	1σ	$^{206}Pb/^{238}U$	1σ
13	569	747	838	0.76	0.96	0.1728	0.0007	11.745	0.095	0.4933	0.0032	2585	6	2584	8	2585	14
14	332	343	312	0.97	1.94	0.1675	0.0007	9.792	0.076	0.4236	0.0025	2533	6	2415	7	2277	11
15	803	945	862	0.85	1.86	0.1672	0.0011	7.866	0.132	0.3416	0.0036	2530	15	2216	15	1894	17
16	847	1239	889	0.68	1.97	0.1668	0.001	10.766	0.175	0.4682	0.0051	2526	14	2503	15	2476	22
17	953	1235	154	0.77	2.03	0.1667	0.0007	10.965	0.115	0.4786	0.0036	2525	9	2520	10	2521	16
18	846	641	521	1.32	1.98	0.1705	0.0008	11.775	0.096	0.5012	0.0032	2563	6	2587	8	2619	14
19	686	742	866	0.92	1.95	0.1692	0.0006	11.326	0.078	0.4852	0.0028	2550	5	2550	6	2550	12
20	1224	1817	115	0.67	1.97	0.1691	0.0008	11.278	0.095	0.4836	0.0032	2549	7	2546	8	2543	14
21	980	1413	1354	0.69	2.02	0.1675	0.001	10.813	0.167	0.4685	0.0046	2533	14	2507	14	2477	20
22	231	293	602	0.79	1.98	0.1673	0.0008	11.172	0.133	0.4845	0.0041	2531	10	2538	11	2547	18
23	689	1038	963	0.66	1.97	0.1672	0.0006	10.951	0.105	0.4746	0.0033	2530	8	2519	9	2504	14
24	326	331	629	0.98	1.96	0.1695	0.0007	11.418	0.082	0.4883	0.0028	2553	6	2558	7	2563	12
25	822	783	1076	1.05	2.06	0.1698	0.0006	11.142	0.091	0.4762	0.0031	2556	6	2535	8	2511	14
MWY02						**Isotopic**	**ratios**					**Age (Ma)**					
Spot	Th	U	Pb	Th/U	$^{238}U/^{232}Th$	$^{207}Pb/^{206}Pb$	1σ	$^{207}Pb/^{235}U$	1σ	$^{206}Pb/^{238}U$	1σ	$^{207}Pb/^{206}Pb$	1σ	$^{207}Pb/^{235}U$	1σ	$^{206}Pb/^{238}U$	1σ
1	127	163	173	0.78	3.32	0.1662	0.0006	10.985	0.092	0.4796	0.0032	2520	6	2522	8	2526	14
2	1103	1405	1814	0.79	3.32	0.1665	0.0007	10.692	0.121	0.4658	0.0035	2523	10	2497	11	2465	15
3	204	193	226	1.06	3.33	0.1667	0.0008	10.913	0.125	0.4746	0.0038	2525	9	2516	11	2504	17
4	468	642	769	0.73	3.32	0.1665	0.0005	10.271	0.071	0.4478	0.0026	2523	5	2459	6	2385	12
5	326	2843	364	0.11	1.24	0.1053	0.0005	3.385	0.025	0.173	0.0008	1720	7	1501	6	1029	4
6	185	128	172	1.45	3.33	0.1643	0.0009	10.486	0.184	0.4636	0.0051	2500	16	2479	16	2455	22
7	378	265	334	1.43	3.33	0.1641	0.0006	10.792	0.113	0.4776	0.0036	2498	9	2505	10	2517	16
8	1805	1139	1438	1.58	3.32	0.1642	0.0007	10.782	0.093	0.4762	0.0032	2499	7	2505	8	2511	14
9	172	188	215	0.91	3.32	0.1641	0.0008	9.957	0.106	0.4405	0.0034	2498	9	2431	10	2353	15
10	251	327	337	0.77	3.32	0.1636	0.0006	9.695	0.093	0.4295	0.0031	2493	8	2406	9	2303	14
11	644	626	725	1.03	3.33	0.1668	0.0008	10.996	0.154	0.4786	0.0043	2526	12	2523	13	2521	19
12	1015	1566	1429	0.65	3.32	0.1663	0.0011	10.937	0.185	0.4775	0.0051	2521	15	2518	16	2516	22
13	362	462	453	0.78	3.33	0.1668	0.0008	10.984	0.162	0.4783	0.0045	2526	13	2522	14	2520	20
14	406	516	455	0.79	3.32	0.1638	0.0008	10.548	0.106	0.4675	0.0032	2495	8	2484	9	2473	14
15	408	475	542	0.86	6.58	0.1662	0.0007	10.961	0.135	0.4785	0.0045	2520	10	2520	11	2521	20
16	1243	1842	2473	0.67	2.06	0.1645	0.0008	10.763	0.096	0.4752	0.0032	2502	7	2503	8	2506	14
17	652	756	117	0.86	6.64	0.1663	0.0007	10.922	0.134	0.4766	0.0042	2521	10	2517	11	2512	18
18	476	466	568	1.02	2.09	0.1661	0.0008	10.936	0.138	0.4782	0.0023	2519	15	2518	12	2519	10
19	1525	2213	2314	0.69	1.98	0.1638	0.0008	7.624	0.063	0.3378	0.0036	2495	8	2188	7	1876	17
20	994	1352	2135	0.74	6.76	0.1638	0.0007	10.678	0.123	0.4726	0.0035	2495	10	2496	11	2495	15
21	801	781	1253	1.03	1.92	0.1786	0.0008	11.652	0.118	0.4733	0.0035	2640	8	2577	9	2498	15
22	422	512	43	0.82	6.57	0.1638	0.0007	10.583	0.116	0.4685	0.0056	2495	9	2487	10	2477	25
23	2674	4015	4655	0.67	6.63	0.1774	0.0008	11.923	0.212	0.4871	0.0041	2629	18	2598	17	2558	18

(*Continued*)

https://doi.org/10.1017/S0016756822000784 Published online by Cambridge University Press

Table 1. (*Continued*)

MWY02						Isotopic	ratios					Age (Ma)					
Spot	Th	U	Pb	Th/U	$^{238}U/^{232}Th$	$^{207}Pb/^{206}Pb$	1σ	$^{207}Pb/^{235}U$	1σ	$^{206}Pb/^{238}U$	1σ	$^{207}Pb/^{206}Pb$	1σ	$^{207}Pb/^{235}U$	1σ	$^{206}Pb/^{238}U$	1σ
24	586	785	61	0.75	6.65	0.1642	0.0008	10.627	0.135	0.4703	0.0033	2499	12	2491	12	2485	14
25	972	1351	1767	0.72	6.63	0.1641	0.0007	10.618	0.136	0.4705	0.0034	2498	12	2490	12	2486	15
26	2473	3015	3408	0.82	1.96	0.1639	0.0009	7.628	0.631	0.3376	0.0035	2496	127	2188	74	1875	17
ZJY01						**Isotopic**	**ratios**					**Age (Ma)**					
Spot	Th	U	Pb	Th/U	$^{238}U/^{232}Th$	$^{207}Pb/^{206}Pb$	1σ	$^{207}Pb/^{235}U$	1σ	$^{206}Pb/^{238}U$	1σ	$^{207}Pb/^{206}Pb$	1σ	$^{207}Pb/^{235}U$	1σ	$^{206}Pb/^{238}U$	1σ
1	123	166	169	0.74	3.33	0.1662	0.0006	10.985	0.092	0.4796	0.0032	2520	6	2522	8	2526	14
2	1085	1409	1811	0.77	3.33	0.1665	0.0007	10.692	0.121	0.4658	0.0035	2523	10	2497	11	2465	15
3	202	197	224	1.03	3.32	0.1667	0.0008	10.913	0.125	0.4746	0.0038	2525	9	2516	11	2504	17
4	465	649	766	0.72	3.33	0.1665	0.0005	10.271	0.071	0.4478	0.0026	2523	5	2459	6	2385	12
5	187	131	168	1.43	3.33	0.1643	0.0009	10.486	0.184	0.4636	0.0051	2500	16	2479	16	2455	22
6	375	272	330	1.38	3.33	0.1641	0.0006	10.792	0.113	0.4776	0.0036	2498	9	2505	10	2517	16
7	1798	1146	1434	1.57	3.33	0.1642	0.0007	10.782	0.093	0.4762	0.0032	2499	7	2505	8	2511	14
8	167	191	211	0.87	3.33	0.1641	0.0008	9.957	0.106	0.4405	0.0034	2498	9	2431	10	2353	15
9	249	330	334	0.75	3.32	0.1636	0.0006	9.695	0.093	0.4295	0.0031	2493	8	2406	9	2303	14
10	640	635	722	1.01	3.33	0.1668	0.0008	10.996	0.154	0.4786	0.0043	2526	12	2523	13	2521	19
11	992	1604	1431	0.62	3.33	0.1663	0.0011	10.937	0.185	0.4775	0.0051	2521	15	2518	16	2516	22
12	357	470	451	0.76	3.32	0.1668	0.0008	10.984	0.162	0.4783	0.0045	2526	13	2522	14	2520	20
13	401	528	452	0.76	3.33	0.1638	0.0008	10.548	0.106	0.4675	0.0032	2495	8	2484	9	2473	14
14	403	482	537	0.84	6.56	0.1662	0.0007	10.961	0.135	0.4785	0.0045	2520	10	2520	11	2521	20
15	1235	1873	2466	0.66	2.05	0.1645	0.0008	10.763	0.096	0.4752	0.0032	2502	7	2503	8	2506	14
16	648	769	115	0.84	6.62	0.1663	0.0007	10.922	0.134	0.4766	0.0042	2521	10	2517	11	2512	18
17	470	488	563	0.96	2.07	0.1661	0.0008	10.936	0.138	0.4782	0.0023	2519	15	2518	12	2519	10
18	1518	2412	2299	0.63	1.96	0.1638	0.0008	7.624	0.063	0.3378	0.0036	2495	8	2188	7	1876	17
19	985	1382	2129	0.71	6.74	0.1638	0.0007	10.678	0.123	0.4726	0.0035	2495	10	2496	11	2495	15
20	793	805	1249	0.98	1.88	0.1786	0.0008	11.652	0.118	0.4733	0.0035	2640	8	2577	9	2498	15
21	417	530	37	0.79	6.54	0.1638	0.0007	10.583	0.116	0.4685	0.0056	2495	9	2487	10	2477	25
22	2665	4049	4660	0.66	6.58	0.1774	0.0008	11.923	0.212	0.4871	0.0041	2629	18	2598	17	2558	18
23	584	801	54	0.73	6.63	0.1642	0.0008	10.627	0.135	0.4703	0.0033	2499	12	2491	12	2485	14
24	966	1362	1758	0.71	6.58	0.1641	0.0007	10.618	0.136	0.4705	0.0034	2498	12	2490	12	2486	15
25	2469	3172	3392	0.78	1.94	0.1639	0.0009	7.628	0.631	0.3376	0.0035	2496	127	2188	74	1875	17

up to 1100 °C for 1 h. Trace element analysis was performed with an ELAN 6000 ICP-MS at the SKLDG, following procedures described by Qi *et al.* (2000). The discrepancy between triplicate analyses is less than 5 % for all elements. Analyses of international standards OU-6 and GBPG-1 are in good agreement with recommended values (Table 3). During Rb–Sr and Sm–Nd isotopic analysis, the sample powder was added with mixed isotopic tracer and dissolved in a polytetrafluoroethylene capsule with HF + HNO_3 (Zhang *et al.* 2001). Isotopic measurements were performed using a Finnigan Triton Ti thermal ionization mass spectrometer at the SKLDG. Procedural blanks yielded concentrations of <200 pg for Sm and Nd and <500 pg for Rb and Sr, and mass fractionation corrections for Sr–Nd isotopic ratios were based on $^{86}Sr/^{88}Sr = 0.1194$ and $^{146}Nd/^{144}Nd = 0.7219$, respectively. Analysis of the NBS987 and La Jolla standards yielded values of $^{87}Sr/^{86}Sr = 0.710246 \pm 16$ (2σ), and $^{143}Nd/^{144}Nd = 0.511863 \pm 8$ (2σ), respectively.

4. Results

4.a. Zircon U–Pb ages

Euhedral zircons in samples WJA1, WJB3, MWY2 and ZJY1 are clean and prismatic and show clear oscillatory magmatic zoning

https://doi.org/10.1017/S0016756822000784 Published online by Cambridge University Press

Table 2. Major element concentrations (wt %) for the mafic dykes studied. LOI = loss on ignition; $Mg^{\#}$ = 100Mg/(Mg + Fe) in atomic proportions; RV = recommended values; MV=measured values. Values for GSR-1 and GSR-3 are from Wang *et al.* (2003)

Sample	Rock type	SiO_2	TiO_2	Al_2O_3	Fe_2O_3	MnO	MgO	CaO	Na_2O	K_2O	P_2O_5	LOI	Total	$Mg^{\#}$
WJA1	dolerite	52.16	0.35	20.43	8.42	0.25	4.36	5.75	3.78	3.28	0.31	0.35	99.44	53
WJA2	dolerite	52.13	0.34	20.45	8.41	0.26	4.38	5.76	3.76	3.27	0.28	0.41	99.45	53
WJA3	dolerite	52.15	0.35	20.73	8.34	0.25	4.36	5.58	3.78	3.25	0.28	0.28	99.35	54
WJA4	dolerite	52.24	0.35	20.66	8.38	0.23	4.38	5.65	3.65	3.25	0.35	0.33	99.47	53
WJA5	dolerite	52.18	0.36	20.68	8.55	0.22	4.36	5.64	3.62	3.25	0.35	0.34	99.55	53
WJA6	dolerite	52.15	0.36	20.66	8.52	0.18	4.34	5.63	3.56	3.26	0.36	0.43	99.45	53
WJA7	dolerite	52.15	0.35	20.38	8.66	0.26	4.38	5.72	3.75	3.32	0.25	0.26	99.48	53
WJA8	dolerite	52.11	0.35	20.55	8.75	0.19	4.35	5.55	3.56	3.26	0.38	0.38	99.43	52
WJB1	dolerite	52.29	0.36	20.62	8.76	0.18	4.35	5.63	3.55	3.25	0.38	0.19	99.56	52
WJB2	dolerite	52.27	0.26	20.26	8.86	0.22	4.34	5.61	3.76	3.28	0.28	0.37	99.51	52
WJB3	dolerite	52.28	0.31	20.25	8.85	0.21	4.36	5.62	3.78	3.25	0.26	0.34	99.51	52
WJB4	dolerite	52.36	0.32	20.65	8.65	0.23	4.34	5.61	3.69	3.31	0.28	0.22	99.66	52
WJB5	dolerite	52.29	0.33	20.28	8.76	0.24	4.38	5.66	3.77	3.28	0.32	0.29	99.60	52
WJB6	dolerite	52.35	0.35	20.56	8.65	0.23	4.35	5.58	3.66	3.28	0.28	0.24	99.53	53
WJB7	dolerite	52.26	0.34	20.68	8.63	0.18	4.36	5.54	3.65	3.34	0.29	0.35	99.62	53
WJB8	dolerite	52.14	0.33	20.66	8.65	0.21	4.32	5.55	3.65	3.29	0.28	0.42	99.50	52
MWY1	dolerite	52.12	0.28	20.31	8.68	0.23	4.35	5.66	3.79	3.26	0.28	0.52	99.48	52
MWY2	dolerite	52.14	0.34	20.65	8.65	0.25	4.35	5.53	3.65	3.26	0.35	0.36	99.53	53
MWY3	dolerite	52.16	0.35	20.32	8.75	0.24	4.35	5.65	3.78	3.25	0.25	0.35	99.45	52
MWY4	dolerite	52.21	0.35	20.68	8.55	0.18	4.36	5.56	3.67	3.26	0.29	0.43	99.54	53
MWY5	dolerite	52.29	0.34	20.42	8.55	0.25	4.38	5.68	3.77	3.33	0.28	0.31	99.60	53
MWY6	dolerite	52.13	0.36	20.76	8.53	0.25	4.36	5.55	3.74	3.28	0.25	0.34	99.55	53
MWY7	dolerite	52.12	0.36	20.36	8.52	0.26	4.38	5.76	3.76	3.35	0.32	0.37	99.56	53
ZJY1	dolerite	52.16	0.37	20.45	8.58	0.26	4.06	5.64	3.76	3.26	0.29	0.44	99.27	52
ZJY2	dolerite	52.15	0.36	20.72	8.46	0.19	4.05	5.53	3.58	3.25	0.35	0.54	99.18	55
ZJY3	dolerite	52.16	0.28	20.46	8.55	0.23	4.03	5.53	3.75	3.33	0.28	0.58	99.18	54
ZJY4	dolerite	52.17	0.35	20.75	8.53	0.22	4.07	5.52	3.53	3.25	0.32	0.44	99.15	54
ZJY5	dolerite	52.22	0.36	20.69	8.38	0.23	4.06	5.53	3.56	3.28	0.35	0.51	99.17	55
ZJY6	dolerite	52.16	0.26	20.46	8.53	0.22	4.08	5.56	3.72	3.36	0.32	0.63	99.30	53
ZJY7	dolerite	52.13	0.26	20.68	8.35	0.24	4.05	5.64	3.93	3.28	0.26	0.45	99.27	56
GSR-3	RV	44.63	2.37	13.83	13.4	0.17	7.77	8.81	3.38	2.32	0.95		97.63	
GSR-3	MV	44.74	2.36	14.14	13.35	0.16	7.74	8.82	3.18	2.30	0.97		97.76	
GSR-1	RV	72.82	0.29	13.42	2.14	0.06	0.42	1.55	3.13	5.01	0.09		98.93	
GSR-1	MV	72.65	0.29	13.52	2.18	0.06	0.46	1.56	3.15	5.03	0.11		99.01	

(Fig. 3). Twenty-three zircon grains from sample WJA1 yielded a weighted mean $^{206}Pb/^{238}U$ age of 2523 ± 7.7 Ma (1σ, 95 % confidence interval; Table 1; Fig. 4a) and weighted mean $^{207}Pb/^{206}Pb$ age of 2538 ± 3.2 Ma (2σ, 95 % confidence interval; Table 1; Fig. 4e). Twenty-five zircon grains from sample WJB3 yielded a weighted mean $^{206}Pb/^{238}U$ age of 2509 ± 7.7 Ma (1σ, 95 % confidence interval; Table 1; Fig. 4b), and weighted mean $^{207}Pb/^{206}Pb$ age of 2510 ± 6.1 Ma (2σ, 95 % confidence interval; Table 1; Fig. 4f). Twenty-five zircon grains from sample MWY2 yielded a weighted mean $^{206}Pb/^{238}U$ age of 2512 ± 12 Ma (1σ, 95 % confidence interval; Table 1; Fig. 4c) and weighted mean $^{207}Pb/^{206}Pb$ age of 2509 ± 6.2 Ma (2σ, 95 % confidence interval; Table 1; Fig. 4g). Twenty-four zircon grains from sample ZJY1 yielded a weighted mean $^{206}Pb/^{238}U$ age of 2539 ± 6.5 Ma (1σ, 95 % confidence interval; Table 1; Fig. 4d) and weighted mean $^{207}Pb/^{206}Pb$ age of 2537 ± 6.2 Ma (2σ, 95 % confidence interval; Table 1; Fig. 4h). These age data provide the best estimates of the crystallization ages of dykes ($^{207}Pb/^{206}Pb$ weighted average *c.* 2.5 Ga) within the study

https://doi.org/10.1017/S0016756822000784 Published online by Cambridge University Press

https://doi.org/10.1017/S0016756822000784 Published online by Cambridge University Press

Table 3. Trace element compositions (ppm) of the mafic dykes studied. RV = recommended values; MV = measured values. Values for GBPG-1 and OU-6 are from Thompson *et al.* (2000) and Potts and Kane (2005), respectively.

Sample	WJA1	WJA2	WJA3	WJA4	WJA5	WJA6	WJA7	WJA8	WJB1	WJB2	WJB3	WJB4	WJB5	WJB6	WJB7	WJB8	MWY1
Cr	155	162	133	164	155	165	185	126	218	192	208	197	206	268	195	166	165
Ni	68.5	53.6	58.3	56.5	53.4	55.3	57.5	44.6	67.2	62.5	56.5	52.4	43.3	88.2	56.5	55.2	51.3
Rb	86.4	98.7	68.6	78.5	76.2	92.4	116	82.3	76.4	63.6	132	63.5	128	124	116	131	95.8
Sr	696	842	664	915	856	735	798	565	732	823	645	746	885	622	765	592	746
Y	11.6	12.5	15.6	12.2	12.3	11.2	15.6	16.3	16.4	15.8	16.9	16.3	18.8	16.9	16.7	12.7	14.5
Zr	118	123	114	121	124	117	127	113	126	125	134	135	142	139	141	143	146
Nb	4.93	4.45	5.23	4.36	5.05	4.32	5.46	4.57	4.83	4.96	6.98	6.65	7.13	5.49	6.86	6.15	6.45
Ba	956	2075	885	1125	1021	1062	683	645	2912	826	838	534	319	842	1043	896	913
La	21.8	21.4	24.6	23.3	26.1	21.3	25.8	27.6	27.5	24.6	24.5	17.6	26.6	24.4	23.1	24.2	27.3
Ce	34.6	32.5	37.8	36.6	38.6	33.3	45.3	41.5	44.4	42.3	47.8	32.3	48.1	45.7	37.9	38.8	44.5
Pr	3.97	4.06	4.57	4.42	4.65	3.89	5.45	5.13	5.31	4.96	5.95	4.85	5.93	5.76	5.29	4.31	4.95
Nd	14.9	15.6	18.3	17.1	17.2	14.9	19.6	19.5	20.8	19.6	21.5	18.8	21.3	21.5	19.9	15.6	18.5
Sm	3.22	3.54	4.15	3.56	3.58	3.17	4.18	4.34	4.56	4.28	4.42	4.19	4.74	4.36	4.45	3.41	3.81
Eu	0.93	1.02	1.16	1.05	1.06	0.95	1.18	1.26	1.25	1.23	1.28	1.12	1.35	1.25	1.25	0.95	1.06
Gd	2.42	2.81	3.35	2.72	2.63	2.52	3.15	3.45	3.71	3.38	3.53	3.44	4.03	3.55	3.55	2.55	2.95
Tb	0.34	0.46	0.46	45	0.38	0.35	0.48	0.53	0.47	0.48	0.53	0.51	0.58	0.53	0.52	0.38	0.45
Dy	1.76	1.98	2.58	1.98	2.03	1.85	2.47	2.68	2.54	2.52	2.58	2.58	3.02	2.63	2.73	2.06	2.28
Ho	0.36	0.43	0.55	0.44	0.45	0.38	0.55	0.55	0.52	0.53	0.55	0.53	0.65	0.55	0.55	0.43	0.45
Er	0.96	1.09	1.38	1.08	1.07	0.97	1.39	1.42	1.41	1.42	1.42	1.36	1.63	1.41	1.43	1.13	1.26
Tm	0.14	0.15	0.18	0.15	0.14	0.14	0.18	0.19	0.18	0.19	0.18	0.19	0.21	0.18	0.19	0.16	0.16
Yb	0.86	0.98	1.21	0.94	0.97	0.89	1.25	1.26	1.24	1.19	1.28	1.26	1.42	1.32	1.31	1.03	1.13
Lu	0.13	0.14	0.15	0.15	0.13	0.14	0.17	0.17	0.18	0.17	0.18	0.19	0.19	0.18	0.18	0.13	0.18
Hf	2.36	2.38	2.33	2.42	2.52	2.42	2.63	2.25	2.44	2.46	2.65	2.66	2.76	2.74	2.77	2.84	2.95
Ta	2.16	0.33	0.31	0.36	1.41	0.89	0.34	0.31	0.26	0.42	0.71	0.76	0.92	4.83	0.52	0.18	0.43
Pb	30.3	16.5	17.5	24.4	25.5	16.3	16.5	16.3	30.2	20.5	22.4	12.5	22.5	21.8	21.5	26.5	14.2
Th	2.52	2.76	3.25	2.75	2.84	2.61	8.15	2.95	3.59	4.65	5.06	5.21	3.72	5.25	4.96	3.75	4.28
U	1.36	1.12	1.05	1.16	1.19	1.15	1.76	1.23	1.31	1.52	1.95	2.21	2.43	1.92	2.36	2.13	2.18
$(La/Yb)_N$	18.2	15.7	14.6	17.8	19.3	17.2	14.8	15.7	15.9	14.8	13.7	10.0	13.4	13.3	12.6	16.9	17.3
Eu/Eu*	0.98	0.96	0.92	0.99	1.00	0.99	0.95	0.96	0.90	0.95	0.96	0.88	0.92	0.94	0.93	0.94	0.93

MWY2	MWY3	MWY4	MWY5	MWY6	MWY7	ZJY1	ZJY2	ZJY3	ZJY4	ZJY5	ZJY6	ZJY7	OU-6 (RV)	OU-6 (MV)	GBPG-1 (RV)	GBPG-1 (MV*)
198	183	184	74.6	215	72.5	324	206	208	314	266	215	76.8	70.8	73.5	181	187
59.6	50.8	51.2	69.7	88.6	72.3	105	90.6	103	105	112	95.5	75.6	39.8	42.5	59.6	60.6

(*Continued*)

https://doi.org/10.1017/S0016756822000784 Published online by Cambridge University Press

Table 3. (*Continued*)

245	184	186	26.5	57.5	33.4	29.2	36.3	35.4	73.6	26.5	32.7	26.5	120	122	56.2	61.4
748	855	876	634	635	576	547	635	642	525	516	633	626	131	136	364	377
18.4	15.6	17.1	19.9	15.2	12.5	13.7	14.3	13.8	14.7	16.8	13.9	17.2	27.4	26.2	26.2	18.0
135	134	142	105	155	103	118	153	136	114	102	134	92.4	174	183	183	232
5.95	5.98	6.45	5.12	5.66	4.14	4.15	5.63	4.92	4.69	5.28	5.36	4.27	14.8	15.3	9.93	8.74
1435	665	917	482	838	643	585	765	769	741	525	782	546	477	486	908	921
29.2	25.4	27.1	24.8	25.3	19.2	21.3	23.5	23.6	22.2	22.3	23.1	23.6	33.0	33.1	53.0	51.0
46.3	48.9	46.8	43.7	34.3	31.1	31.7	33.5	32.8	28.4	35.2	32.8	36.9	74.4	78.0	103	105
5.78	5.96	5.81	6.13	4.16	3.83	4.29	3.95	4.12	3.74	4.76	4.05	4.89	7.8	8.09	11.5	11.6
21.6	21.8	21.9	24.5	15.6	15.1	16.9	15.3	16.3	14.5	19.6	15.4	19.3	29	30.6	43.3	42.4
4.67	4.45	4.58	5.36	3.46	3.08	3.83	3.24	3.34	3.46	4.45	3.25	4.15	5.92	5.99	6.79	6.63
1.24	1.22	1.35	1.43	1.16	0.98	1.05	1.15	1.23	1.08	1.17	1.15	1.15	1.36	1.35	1.79	1.69
3.56	3.25	3.46	4.18	3.04	2.53	3.05	2.69	2.75	2.95	3.66	2.72	3.25	5.27	5.5	4.74	4.47
0.55	0.53	0.55	0.58	0.41	0.35	0.45	0.43	0.42	0.45	0.52	0.38	0.51	0.85	0.83	0.60	0.59
2.86	2.46	2.65	3.23	2.26	1.85	2.18	2.08	2.13	2.26	2.76	2.06	2.56	4.99	5.06	3.26	3.17
0.61	0.53	0.55	0.65	0.46	0.42	0.46	0.45	0.45	0.47	0.56	0.46	0.55	1.01	1.02	0.69	0.66
1.63	1.43	1.46	1.76	1.28	1.06	1.21	1.25	1.16	1.26	1.45	1.22	1.45	2.98	3.07	2.01	2.02
0.21	0.18	0.19	0.21	0.17	0.18	0.15	0.15	0.17	0.16	0.18	0.15	0.18	0.44	0.46	0.30	0.29
1.42	1.26	1.34	1.45	1.14	0.96	1.05	1.05	1.08	1.15	1.21	1.06	1.29	3.00	3.09	2.03	2.03
0.19	0.18	0.19	0.21	0.18	0.15	0.13	0.15	0.16	0.16	0.17	0.17	0.18	0.45	0.47	0.31	0.31
2.72	2.74	2.83	2.04	2.96	2.05	2.35	2.81	2.92	2.55	2.23	2.85	2.03	4.70	4.86	6.07	5.93
1.12	0.75	0.72	0.95	0.63	0.33	0.26	2.21	0.31	1.74	0.45	0.59	0.25	1.06	1.02	0.40	0.46
7.45	13.8	22.4	13.5	11.5	1.6	23.2	37.5	16.2	22.3	9.76	25.3	15.3	28.2	32.7	14.1	14.5
4.43	4.95	4.96	2.45	4.15	1.95	2.55	4.21	4.56	3.42	2.83	4.46	2.41	11.5	13.9	11.2	11.4
1.92	2.15	1.97	1.26	1.43	1.14	1.22	1.43	1.56	1.03	1.12	1.42	1.23	1.96	2.19	0.90	0.99
14.8	14.5	14.5	12.3	15.9	14.3	14.6	16.1	15.7	13.8	13.2	15.6	13.1				
0.89	0.94	1.00	0.89	1.07	1.04	0.91	1.20	1.20	1.00	0.90	1.20	0.92				

Table 4. Sr–Nd isotopic compositions of the mafic dykes studied. The compositions were calculated using Chondrite Uniform Reservoir values and decay constants of $\lambda_{Rb} = 1.42 \times 10^{-11}$ year^{-1} (Steiger & Jäger, 1977) and $\lambda_{Sm} = 6.54 \times 10^{-12}$ year^{-1} (Lugmair & Harti, 1978)

Sample	Rb (ppm)	Sr (ppm)	$^{87}Rb/^{86}Sr$	$^{87}Sr/^{86}Sr$	± 2δ	Sm (ppm)	Nd (ppm)	$^{147}Sm/^{144}Nd$	$^{143}Nd/^{144}Nd$	± 2δ	$(^{87}Sr/^{86}Sr)_i$	$(^{143}Nd/^{144}Nd)_i$	$\epsilon_{Nd}(t)$
WJA1	188	123	4.4233	0.858261	12	3.48	14.7	0.1425	0.511764	10	0.696914	0.509393	0.5
WJA3	196	135	4.2017	0.850175	13	3.52	14.9	0.1422	0.511742	8	0.696915	0.509376	0.2
WJA4	221	146	4.3806	0.856712	14	3.64	15.6	0.1405	0.511724	12	0.696923	0.509387	0.4
WJA5	256	167	4.4363	0.858735	13	5.16	22.1	0.1406	0.511722	10	0.696916	0.509384	0.4
WJB1	235	153	4.4450	0.858137	14	6.45	28.6	0.1358	0.511647	9	0.696914	0.509401	0.3
WJB2	316	206	4.4393	0.857929	11	7.41	33.1	0.1348	0.511635	8	0.696916	0.509405	0.4
WJB3	216	141	4.4334	0.857714	12	7.97	35.6	0.1348	0.511633	10	0.696917	0.509403	0.4
WJB4	268	175	4.4320	0.857664	13	8.06	36.1	0.1344	0.511625	10	0.702202	0.509401	0.3
MWY1	82.1	736	0.3228	0.713925	12	3.85	18.9	0.1226	0.511435	12	0.702197	0.509404	0.5
MWY2	73.5	658	0.3233	0.713936	13	6.75	33.2	0.1224	0.511436	10	0.702191	0.509409	0.6
MWY3	62.8	562	0.3234	0.713935	12	7.78	38.3	0.1223	0.511437	9	0.702189	0.509411	0.6
MWY5	75.9	679	0.3235	0.713937	14	9.15	45.1	0.1221	0.511438	8	0.702139	0.509415	0.7
ZJY1	76.8	688	0.3231	0.713999	13	7.46	36.7	0.1224	0.511435	10	0.702142	0.509386	0.8
ZJY2	83.5	749	0.3226	0.713986	12	6.83	33.5	0.1227	0.511436	8	0.702156	0.509381	0.7
ZJY3	68.6	616	0.3223	0.713988	14	9.58	47.1	0.1224	0.511425	9	0.702158	0.509375	0.6
ZJY4	75.8	681	0.3221	0.713984	12	6.95	34.2	0.1223	0.511426	10	0.710038	0.509378	0.7

Table 5. Hf isotopic compositions of representative samples studied in western Shandong province

WJA1 Spot	$^{176}Yb/^{177}Hf$	$^{176}Lu/^{177}Hf$	$^{176}Hf/^{177}Hf$	2σ	$\epsilon_{Hf}(t)$	T_{DM1} (Ma)	T_{DM2} (Ma)	$f_{Lu/Hf}$
1	0.040705	0.001563	0.281346	0.000025	3.5	2702	2804	−0.95
2	0.123223	0.003823	0.281278	0.000023	-2.8	2974	3187	−0.95
3	0.067256	0.002456	0.281328	0.000023	1.3	2793	2936	−0.96
4	0.025276	0.001045	0.281313	0.000024	3.2	2711	2821	−0.97
5	0.038623	0.001526	0.281346	0.000023	3.6	2700	2800	−0.95
6	0.159885	0.005046	0.281342	0.000023	-2.6	2983	3176	−0.95
7	0.066172	0.002482	0.281375	0.000025	3.0	2728	2837	−0.95
8	0.031714	0.001261	0.281303	0.000026	2.5	2740	2866	−0.96
9	0.009547	0.000386	0.281322	0.000022	4.7	2653	2733	−0.99
10	0.066406	0.002435	0.281355	0.000025	2.3	2753	2875	−0.93
11	0.016552	0.000641	0.281285	0.000027	2.9	2720	2840	−0.98
12	0.059313	0.002207	0.281304	0.000023	0.9	2808	2962	−0.93
13	0.074368	0.002623	0.281362	0.000022	2.2	2757	2880	−0.95
14	0.017276	0.000723	0.281324	0.000025	4.2	2673	2764	−0.98
15	0.047426	0.001652	0.281324	0.000025	2.6	2739	2861	−0.95
16	0.054484	0.001973	0.281373	0.000025	3.8	2694	2788	−0.94
17	0.025308	0.000992	0.281283	0.000028	2.2	2748	2881	−0.97
18	0.072086	0.002681	0.281316	0.000023	0.5	2827	2986	−0.97
19	0.052124	0.001993	0.281403	0.000026	4.8	2653	2725	−0.94
20	0.018353	0.000852	0.281345	0.000024	4.7	2654	2732	−0.97

(*Continued.*)

https://doi.org/10.1017/S0016756822000784 Published online by Cambridge University Press

Table 5. (*Continued.*)

WJA3								
Spot	$^{176}Yb/^{17}7Hf$	$^{176}Lu/^{177}Hf$	$^{176}Hf/^{177}Hf$	2σ	$\epsilon_{Hf}(t)$	T_{DM1} (Ma)	T_{DM2} (Ma)	$f_{Lu/Hf}$
1	0.159891	0.005044	0.281482	0.000023	2.1	2769	2879	−0.95
2	0.066178	0.002484	0.281365	0.000025	2.3	2743	2866	−0.93
3	0.067258	0.002453	0.281406	0.000023	3.8	2682	2774	−0.96
4	0.025282	0.001043	0.281304	0.000024	2.6	2723	2849	−0.97
5	0.036254	0.001528	0.281343	0.000023	3.1	2704	2815	−0.95
6	0.018357	0.000854	0.281371	0.000024	5.3	2618	2684	−0.97
7	0.016556	0.000645	0.281256	0.000027	1.5	2760	2912	−0.98
8	0.052133	0.001988	0.281345	0.000026	2.4	2734	2858	−0.94
9	0.017279	0.000725	0.281203	0.000025	-0.5	2837	3035	−0.98
10	0.013227	0.003826	0.281425	0.000023	2.1	2758	2876	−0.95
11	0.047432	0.001654	0.281327	0.000025	2.4	2735	2862	−0.95
12	0.054492	0.001975	0.281342	0.000025	2.3	2738	2863	−0.94
13	0.074368	0.002625	0.281333	0.000022	0.9	2799	2950	−0.93
14	0.040711	0.001565	0.281352	0.000025	3.4	2694	2799	−0.95
15	0.031716	0.001263	0.281265	0.000026	0.8	2792	2956	−0.96
16	0.059317	0.002209	0.281366	0.000023	2.8	2721	2836	−0.93
17	0.025311	0.000987	0.281275	0.000028	1.6	2758	2906	−0.97
18	0.072086	0.002683	0.281466	0.000023	5.5	2613	2668	−0.93
MWY2								
Spot	$^{176}Yb/^{17}7Hf$	$^{176}Lu/^{177}Hf$	$^{176}Hf/^{177}Hf$	2σ	$\epsilon_{Hf}(t)$	T_{DM1} (Ma)	T_{DM2} (Ma)	$f_{Lu/Hf}$
1	0.016943	0.000761	0.281406	0.000023	6.8	2565	2596	−0.98
2	0.013574	0.000623	0.281312	0.000025	3.6	2682	2786	−0.98
3	0.009748	0.000434	0.281287	0.000023	3.1	2703	2821	−0.99
4	0.016134	0.000705	0.281309	0.000024	3.4	2692	2801	−0.98
5	0.031293	0.001212	0.281349	0.000023	4.0	2673	2767	−0.96
6	0.015556	0.000665	0.281454	0.000023	8.6	2493	2482	−0.98
7	0.023008	0.000976	0.281243	0.000028	0.6	2801	2972	−0.97
8	0.014312	0.000635	0.281265	0.000023	2.0	2747	2889	−0.98
9	0.032091	0.001276	0.281313	0.000023	2.6	2727	2852	−0.96
10	0.014305	0.000609	0.281352	0.000024	5.1	2628	2698	−0.98
11	0.015567	0.000694	0.281254	0.000027	1.5	2766	2919	−0.98
12	0.013834	0.000615	0.281335	0.000025	4.5	2651	2735	−0.98
13	0.015436	0.000692	0.281321	0.000022	3.8	2675	2774	−0.98
14	0.033412	0.001576	0.281334	0.000025	2.8	2720	2837	−0.95
15	0.021135	0.000828	0.281367	0.000025	5.3	2622	2688	−0.98
16	0.050376	0.001956	0.281324	0.000026	1.8	2761	2899	−0.94
17	0.011546	0.000452	0.281153	0.000025	-1.7	2884	3113	−0.99
18	0.021254	0.000901	0.281257	0.000026	1.2	2777	2934	−0.97
ZJY2								
Spot	$^{176}Yb/^{17}7Hf$	$^{176}Lu/^{177}Hf$	$^{176}Hf/^{177}Hf$	2σ	$\epsilon_{Hf}(t)$	T_{DM1} (Ma)	T_{DM2} (Ma)	$f_{Lu/Hf}$
1	0.023012	0.000983	0.281285	0.000028	2.7	2744	2866	−0.97
2	0.033416	0.001582	0.281345	0.000025	3.8	2705	2799	−0.95

(*Continued*)

https://doi.org/10.1017/S0016756822000784 Published online by Cambridge University Press

Table 5. (*Continued*)

ZJY2 Spot	$^{176}Yb/^{17}7Hf$	$^{176}Lu/^{177}Hf$	$^{176}Hf/^{177}Hf$	2σ	$\epsilon_{Hf}(t)$	T_{DM1} (Ma)	T_{DM2} (Ma)	$f_{Lu/Hf}$
3	0.016945	0.000764	0.281326	0.000023	4.5	2673	2754	−0.98
4	0.013578	0.000625	0.281273	0.000025	2.9	2735	2854	−0.98
5	0.031295	0.001217	0.281372	0.000023	5.4	2642	2702	−0.96
6	0.015562	0.000671	0.281425	0.000023	8.2	2532	2528	−0.98
7	0.013838	0.000621	0.281364	0.000025	6.1	2612	2657	−0.98
8	0.015438	0.000694	0.281334	0.000022	4.9	2658	2729	−0.98
9	0.014309	0.000613	0.281215	0.000024	0.8	2813	2979	−0.98
10	0.015573	0.000697	0.281276	0.000027	2.8	2736	2856	−0.98
11	0.021137	0.000832	0.281352	0.000025	5.3	2643	2705	−0.97
12	0.050379	0.001957	0.281303	0.000026	1.6	2791	2929	−0.94
13	0.011548	0.000454	0.281145	0.000025	-1.4	2895	3114	−0.99
14	0.032095	0.001281	0.281322	0.000023	3.5	2715	2817	−0.96
15	0.021257	0.000904	0.281243	0.000026	1.3	2796	2949	−0.97
16	0.014315	0.000637	0.281279	0.000023	3.1	2728	2843	−0.98
17	0.009752	0.000436	0.281298	0.000023	4.1	2688	2780	−0.99
18	0.016137	0.000709	0.281326	0.000024	4.6	2670	2748	−0.98

area. No major zircon inheritance was observed in any of the samples.

4.b. Major and trace element geochemistry

The dykes studied appear quite evolved and show SiO_2 (52.11–52.36 wt %), TiO_2 (0.26–0.37 wt %), Al_2O_3 (20.25–20.68 wt %), Fe_2O_3 (8.34–8.86 wt %), MnO (0.18–0.26 wt %), MgO (4.03–4.38 wt %), CaO (5.52–5.76 wt %), Na_2O (3.55–3.93 wt %), K_2O (3.23–3.36 wt %) and P_2O_5 (0.25–0.38 wt %) (Table 2). All the dykes studied are classified as alkaline (shoshonites) on the total-alkali silica diagram (Figs. 5a and 6) and as shoshonites in a Na_2O vs K_2O diagram (Figs. 5b and 6). They are characterized by enrichment in $(La/Sm)_N$ (1.57–2.57) and depletion in $(Dy/Yb)_N$ (1.30–1.42), with a variation range in $(La/Yb)_N$ (7.17–8.55), and the Eu/Eu* ratios appears slightly positive (1.12–1.27) (Table 3; Figs. 7 and 8a, b, modified based on comments). Furthermore, the mafic dykes are enriched in Ba, K, Pb, Sr, Eu, Dy and Lu; with negative U, Nb, Ta, Pr, P, Nd and Ti anomalies in primitive-mantle-normalized multi-element variation diagrams (Figs. 7 and 8a, b).

4.c. Whole-rock Sr–Nd and zircon Hf isotopes

The Sr–Nd isotopic compositions of 16 representative dykes were determined (Table 4; Fig. 9). They have a relatively narrow range of $(^{87}Sr/^{86}Sr)_i$ ratios (~0.6969) and have positive $\epsilon_{Nd}(t)$ values (0.2–0.8), implying an isotope-depleted magma source. The mean Nd model age is 2.73 Ga (DePaolo, 1981). The initial isotopic values of Sr are lower than those of BABI (Basaltic Achondrite Best Initial) (0.69899), for two main reasons (1) at least two mantle end elements (depleted mantle and enriched mantle) are involved in the genetic process (Zhou & Armstrong, 1982; Zhi, 1990; Zou *et al.*, 2000); (2) high melting depth, homogeneity of source area and difference in lithosphere thickness (Niu *et al.*, 2011; Ye *et al.*, 2015). The Hf isotopic compositions of zircon from the mafic dykes were also determined (Table 5; Fig. 10). Twenty spot analyses were obtained for sample WJA1, yielding $\varepsilon_{Hf}(t)$ values (−2.8 to 4.8) corresponding to T_{DM1} model ages (2.98–2.65 Ga, mean $T_{DM1} = 2.75$ Ga). Eighteen spot analyses were obtained for sample WJB3, and the results show $\varepsilon_{Hf}(t)$ values (−0.5 to 5.5) corresponding to T_{DM1} model ages (2.8–2.61 Ga, mean $T_{DM1} = 2.73$ Ga). Eighteen spot analyses were obtained for sample MWY2, yielding a range of $\varepsilon_{Hf}(t)$ values (−1.7 to 8.6) corresponding to T_{DM1} model ages (2.88–2.49 Ga, mean $T_{DM1} = 2.70$ Ga). Eighteen spot analyses in zircon grains from sample ZJY2 show $\varepsilon_{Hf}(t)$ values (−1.4 to 8.2) corresponding to T_{DM1} model ages (2.9–2.53 Ga, mean $T_{DM1} = 2.71$ Ga). The mean T_{DM1} of the four zircons is 2.73 Ga, which is similar to the Nd model age.

5. Discussion

Based on zircon geochronology, whole-rock geochemistry and Nd–Hf isotopic evidence, this study reasonably limits the source area of mafic dykes, crustal contamination, fractional crystallization and magmatic evolution.

5.a. Mantle source and the origin

The mafic dykes studied are quite evolved, and the SiO_2 content is quite high (52.11–52.36 wt %; Table 2), implying an ultra-basic source for these rocks. An ultra-basic source is also supported by the relatively high $Mg^{\#}$ values (52–56; Table 1). It is unlikely that

https://doi.org/10.1017/S0016756822000784 Published online by Cambridge University Press

Fig. 2. (Colour online) The field and microscopic photos of the mafic dykes studied. Pl – plagioclase; Cpx – clinopyroxene.

the magma that formed these dykes had any contribution from crustal rocks (Hirajima *et al.* 1990; Zhang *et al.* 1995; Kato *et al.* 1997; Rapp *et al.* 2003), as lower crustal intermediate granulites (Gao *et al.* 1998*a*, *b*) would produce high-Si and low-$Mg^{\#}$ melts. Moreover, the Zr/Nb (10–16) and Rb/Sr ratios (0.04–0.20) of the dykes studied (Table 3) suggest magma derivation from a depleted mantle source (Weaver, 1991). The dykes also show positive but variable $\epsilon_{Nd}(t)$ (0.2–0.8; Table 4) and ϵ_{Hf} (t) values (0.5–8.6), both of which are consistent with derivation from an isotope-depleted mantle (Liu *et al.* 2009). In addition to the evidence outlined above, plots La/Sm vs La, and Sm/Yb vs Sm (Fig. 11a, b) suggest that the magma was sourced from an isotope-depleted garnet–lherzolite mantle through a moderate degree of partial melting (10–20 %). And during the diagenetic process, the separation crystallization mainly occurs with clinopyroxene (Fig. 12). In primitive-mantle-normalized spider plots (Fig. 8b), all the dykes studied show distinct negative anomalies for Nb and Ta, indicating the involvement of crustal components in the mantle source (Zhang *et al.* 2005). The depleted mantle source can be further supported by the zircons from mafic dykes studied, because zircons are obviously recycled and should come from the fusion of depleted mantle sources.

5.b. Crustal contamination

Crustal pollution can lead to the enrichment of Sr–Nd isotopic composition of the basaltic rocks (Guo *et al.* 2004). The positive K, Pb and Zr, negative Nb, Ta and Ti anomalies, low Nb/Ta ratios (3.36–4.88; average 4.18) and relatively uniform La/Nb and higher Ba/Nb ratios (3.5–6.0, 94–466) (Table 3) suggest the contribution of a mantle source related to or contaminated by subducted material (Fig. 8a, b; Guo *et al.* 2013). Although the dolerites studied had a small Sr isotopic composition (~0.6969) and positive $\epsilon_{Nd}(t)$ and $\epsilon_{Hf}(t)$ values (0.2–0.8, 0.5–8.6, except for a few samples), the possibility that the genetic process is affected by crustal contamination cannot be ruled out. In the related diagrams of Nb/Ta vs La/Yb, Ce/Nb vs Th/Nb, Th/Nb vs Ta/Yb and La/Nb vs Ce/Pb (not shown), there are obvious projection laws of the mafic dyke swarms studied, further implying that the genetic process was affected by obvious crustal contamination. The low Ce/Pb (1.64–6.22) and Nb/U ratios (4.38–10.2) and higher La/Nb (1.28–1.65), Zr/Nb (9.97–15.9) and Rb/Nb ratios (2.61–12.3) also imply this. Crustal contamination would result in significant variation in Sr and Nd isotope compositions. Although there is no obvious correlation between MgO and $(^{87}Sr/^{86}Sr)_i$, positive correlations between MgO and $\epsilon_{Nd}(t)$ values are obvious from the dykes

https://doi.org/10.1017/S0016756822000784 Published online by Cambridge University Press

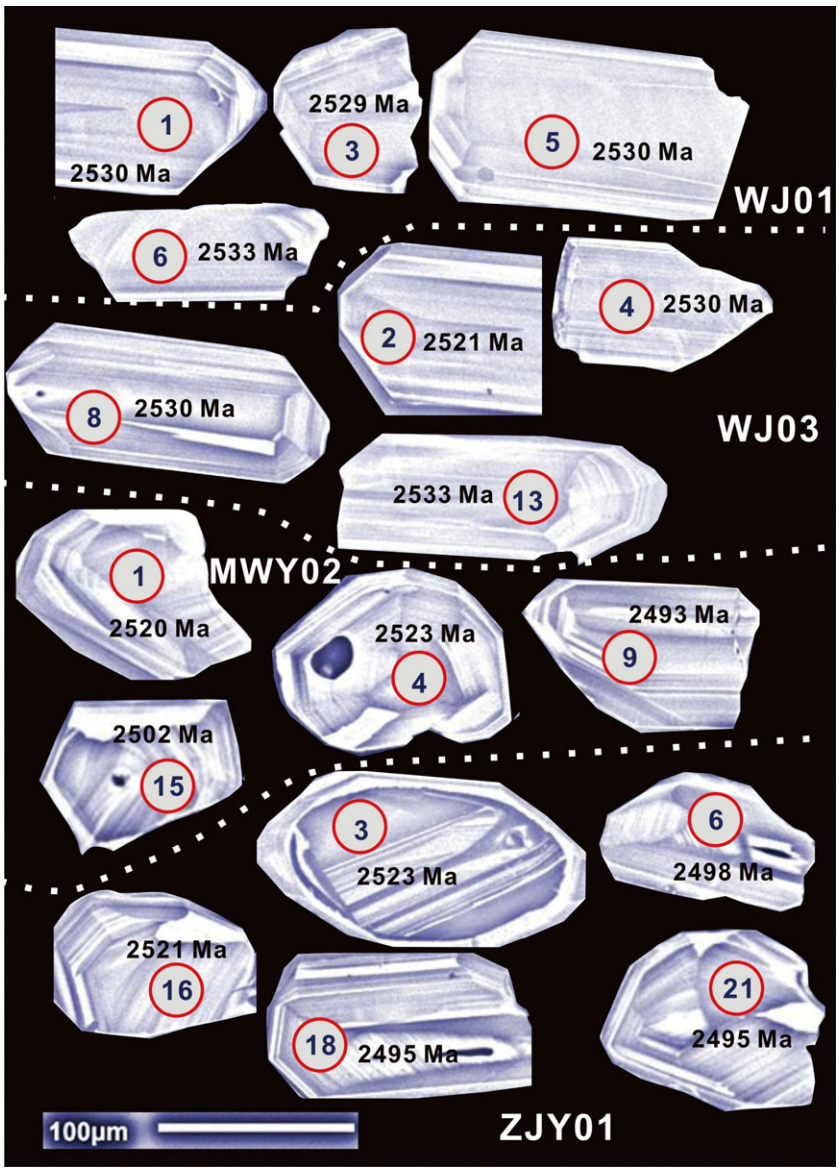

Fig. 3. (Colour online) Representative CL images of zircon grains from samples from the mafic dykes studied.

studied (Fig. 8b; Taylor & McLennan, 1985). Therefore, there was clearly crustal contamination during the formation of these dykesThe mafic dykes are characterized by depletion in Th relative to La (Fig. 8b), eliminating the possibility of significant upper-middle crustal contamination (Taylor & McLennan, 1985). A likely candidate for the contamination might be lower crust.

5.c. Genetic model and tectonic significance

The mafic dykes studied provide possible evidence for the extension of Neoarchaean lithosphere and the evolution of the lower mantle beneath the NCC. Herein, we propose a genetic model of the dykes studied and the tectonic significance.

Geochemical characteristics show that the parent magma forming the mafic dykes comes from the melting of an isotope-depleted garnet lherzolite mantle (10–20 %). However, all the dykes have significant negative high-field-strength elements (HFSE; e.g. Nb, Ta, P and Ti) and positive Pb and K anomalies in the normalized multi-element plots compared to the original mantle (Table 3; Fig. 8a, b). In general, HFSE deficiency (i.e. Nb, Ta) is interpreted as rutile fractionation (Table 3; Fig. 8b; Zhang *et al.* 2005). In addition, the positive anomaly of Pb and K is considered to be the result of mixing and metasomatism of fluids from subducted oceanic plates in the mantle source region (Nelson, 1992; Rogers & Setterfle, 1994; Chung *et al.* 2001; Muller *et al.* 2001).

The high Ba/Nb ratios (51–215; Table 3) of these dykes are different from most intraplate volcanic rocks (i.e. ocean island basalt, alkaline basalt and kimberlite), and their Ba/Nb ratios are very low (from 1.0 to 20; Jahn *et al.* 1999). Therefore, the above data suggest that the mantle-derived magma that generated these has assimilated possible crustal contamination.

Many processes related to plume-related magmatism and mantle chemical heterogeneity (Arndt & Goldstein, 1989; Kay & Kay, 1991; Rudnick & Fountain, 1995; Jull & Kelemen, 2001; Gao *et al.* 2004; Elkins-Tanton, 2005; Lustrino, 2005; Anderson, 2006) are closely related to the subsidence of continental lower crust to convective mantle. As eclogite has higher density than peridotite of lithospheric mantle (Rudnick & Fountain, 1995; Jull & Kelemen, 2001; Anderson, 2006; Levander *et al.* 2006), eclogite material will be easier to recycle into the mantle (Arndt & Goldstein, 1989; Kay

https://doi.org/10.1017/S0016756822000784 Published online by Cambridge University Press

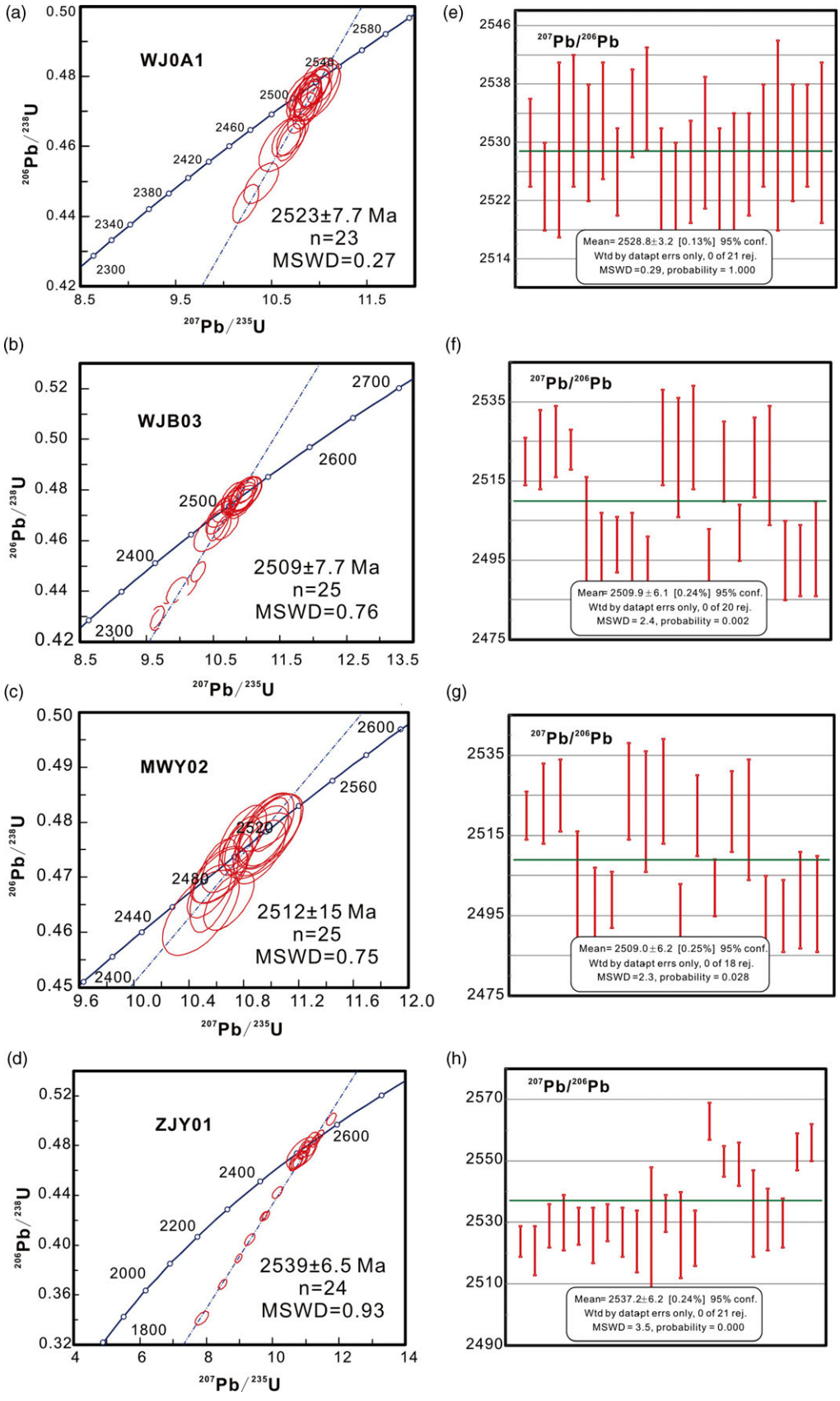

Fig. 4. (Colour online) Zircon LA-ICP-MS U–Pb concordia diagrams and the $^{207}Pb/^{206}Pb$ weighted mean ages from the mafic dykes studied.

https://doi.org/10.1017/S0016756822000784 Published online by Cambridge University Press

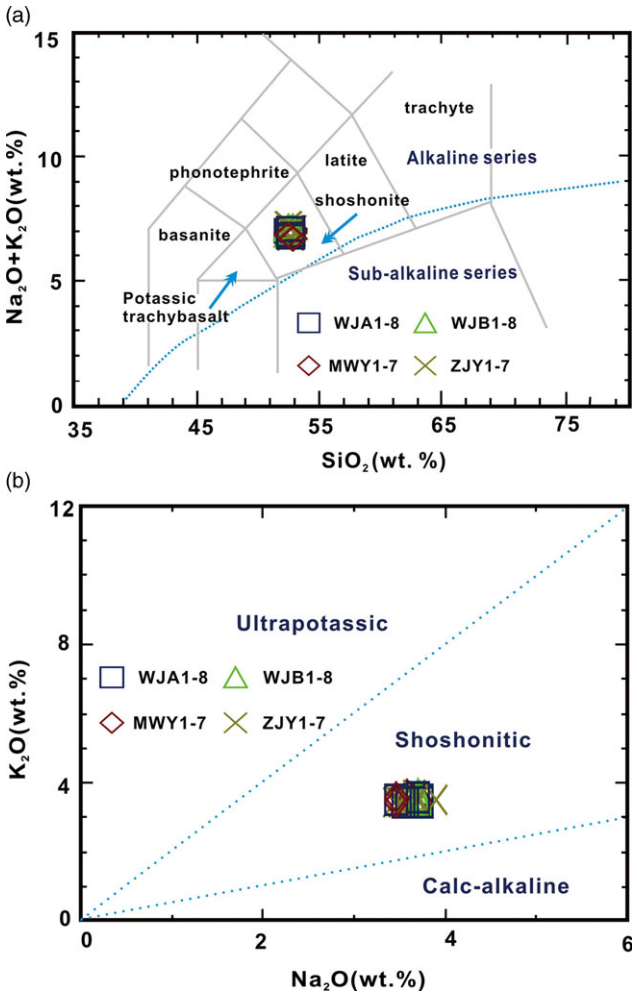

Fig. 5. (Colour online) Classification of the mafic dykes studied. (a) Total-alkali silica (Middlemost, 1994; Le Maitre, 2002) using major element concentrations recalculated to 100 % volatile-free compositions. (b) variations in K_2O vs Na_2O concentrations (Menzies & Kyle, 1972).

& Kay, 1991; Jull & Kelemen, 2001; Gao *et al.* 2004, 2008). Moreover, if the eclogite is silicon-saturated, it can hybridize with the overlying mantle peridotite and produce olivine-free pyroxene. The subsequent melting of these pyroxenes in the mantle can produce basaltic magma (Kogiso *et al.* 2003; Sobolev *et al.* 2005, 2007; Herzberg *et al.* 2007; Gao *et al.* 2008). Therefore, this model has been used to explain the origin of the mafic dyke parent magmas in the NCC (Liu *et al.* 2008*a*, *b*, 2009, 2013*b*).

In general, mafic dyke swarms can provide significant scientific information for the time and stage of extensional tectonics, and are ideal objects for studying mantle plume activity and lithospheric extension (Hou, 2012). Previous studies in the NCC focused on Mesozoic, Cenozoic and Proterozoic mafic dykes and documented three episodes of lithospheric extension during the Proterozoic (i.e. from 1.8 to 1.6 Ga, 1.3 to 1.2 Ga, and 0.8 to 0.7 Ga). Nevertheless, study of the extension of NCC Archaean (age > 2.5 Ga) lithosphere is still very weak (Chen & Shi, 1983, 1994; Chen *et al.* 1992; Shao & Zhang, 2002; Zhang & Sun, 2002; Peng *et al.* 2005, 2007, 2008, 2010, 2011*a*, *b*; Hou *et al.* 2006; Yang *et al.* 2007; Li *et al.* 2010; Peng, 2010). The age data and genetic model in this paper are of considerable significance for basaltic magma activities in the lower crust related to the extension of the Archaean lithosphere. It has been suggested that the large-scale continental accretion and Archaean cratonization (2.5–2.6 Ga) occurred in the southwest and northeast of present-day Shandong province (Wang *et al.* 1999; Hou *et al.* 2004). Generally, the thickened crust will undergo eclogite, and then sink and recycle back to the underlying mantle (Arndt & Goldstein, 1989; Kay & Kay, 1991; Jull & Kelemen, 2001; Gao *et al.* 2004). The foundered eclogite has a higher density than that of the mantle peridotite (Rudnick & Fountain, 1995; Jull & Kelemen, 2001; Anderson, 2006; Levander *et al.* 2006), but its melting temperature is lower than that of mantle peridotite (Yaxley & Green, 1998; Rapp *et al.* 1999; Yaxley, 2000; Kogiso *et al.* 2003; Sobolev *et al.* 2005, 2007). This means that the heating of silicon-saturated eclogite will produce an intermediate acid solution assemblage (from tonalite to

https://doi.org/10.1017/S0016756822000784 Published online by Cambridge University Press

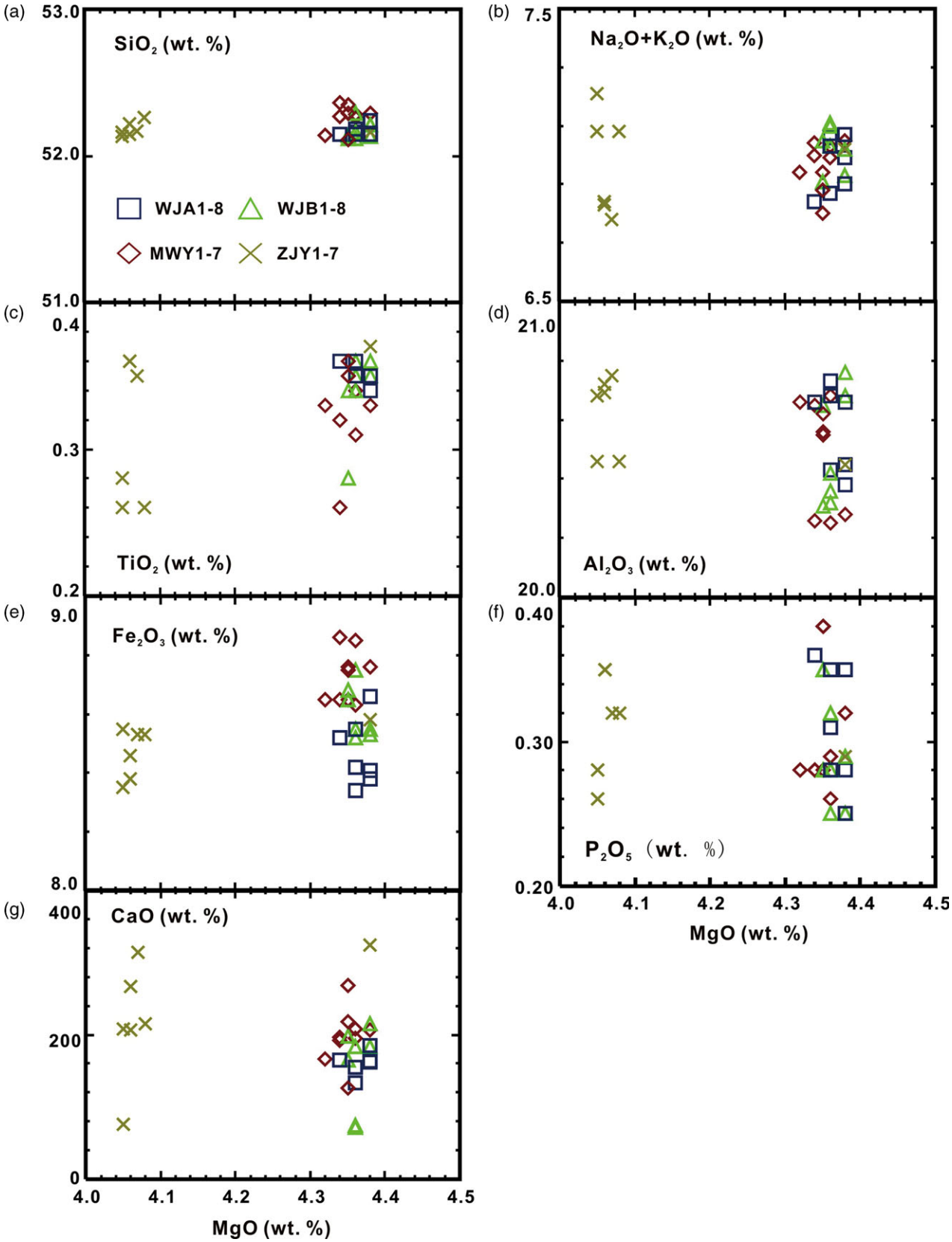

Fig. 6. (Colour online) Variations in major element concentrations vs MgO (wt %) for the mafic dykes studied.

https://doi.org/10.1017/S0016756822000784 Published online by Cambridge University Press

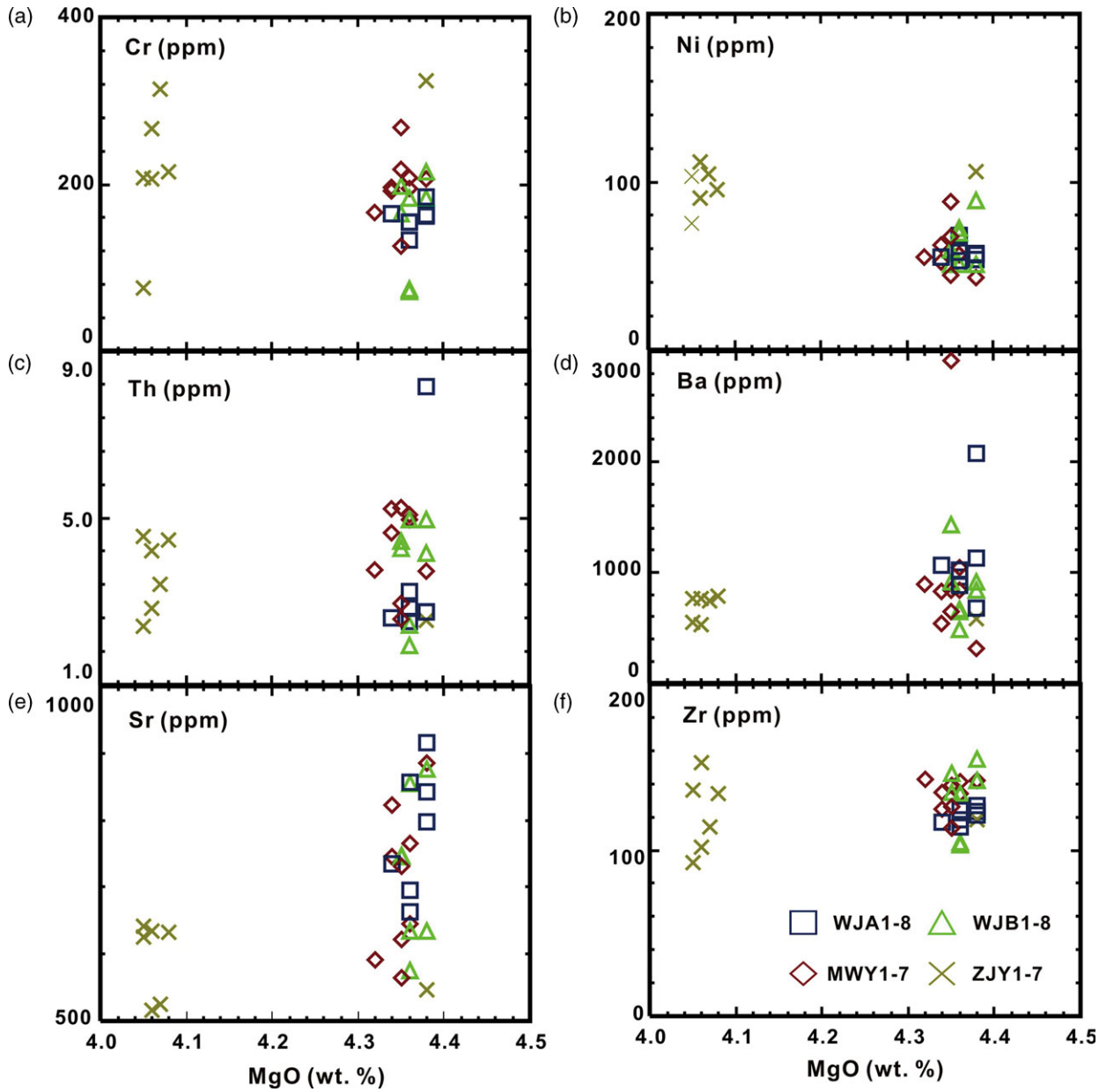

Fig. 7. (Colour online) Variations in trace element concentrations vs MgO (wt %) for the mafic dykes studied.

trondhjemite), rather than basic solution. These melts can be hybridized with mantle peridotite overlying areas to varying degrees. Subsequently, decompression melting of mixed mantle can produce basaltic melt (Kogiso *et al.* 2003; Sobolev *et al.* 2005, 2007; Herzberg *et al.* 2007; Gao *et al.* 2008). Nevertheless, the lithospheric mantle in western Shandong province is not highly enriched, which may be the result of limited hybridization between the mantle and the subsidence lower crust. Subsequently (~2.5 Ga), the partial melting of the slightly mixed mantle will produce the parent magma of the dykes studied. These magmas intruded into the Earth's crust and formed these mafic dykes between ~2.51 Ga and 2.54 Ga. The layered model is further supported by the geochemical composition, which is similar to that of the igneous rocks derived from the layered dynamic model: enrichment in Ba, K, Pb, Sr and Zr, negative HFSE (Nb, Ta and Ti), $(La/Yb)_N$ (7.17–8.55), relatively low $\epsilon_{Nd}(t)$ (0.2–0.8) and $\epsilon_{Hf}(t)$ ratios (−2.8 to 8.6) (Tables 3–5; Figs 7–9; Wedepohl, 1991; Gao *et al.* 1992; Budnick, 1995; Gao & Jin, 1997; Feng *et al.* 2012; Qi *et al.* 2012; Liu *et al.* 2006, 2008*a*, *b*, 2009, 2010*b*, 2010*c*, 2011, 2012*b*, 2013*a*, 2013*c*, 2014, 2015, 2016, 2017, 2018; Luo *et al.* 2006), intense lithosphere thinning (Liu *et al.* 2008*a*, *b*), massive contemporaneous magmatic activity (Regional Geology of Shandong Province, 1995) and large-scale mineralization appear in the NCC (Regional Geology of Shandong Province, 1995). All of the above phenomena can be explained by the foundering of lithosphere.

https://doi.org/10.1017/S0016756822000784 Published online by Cambridge University Press

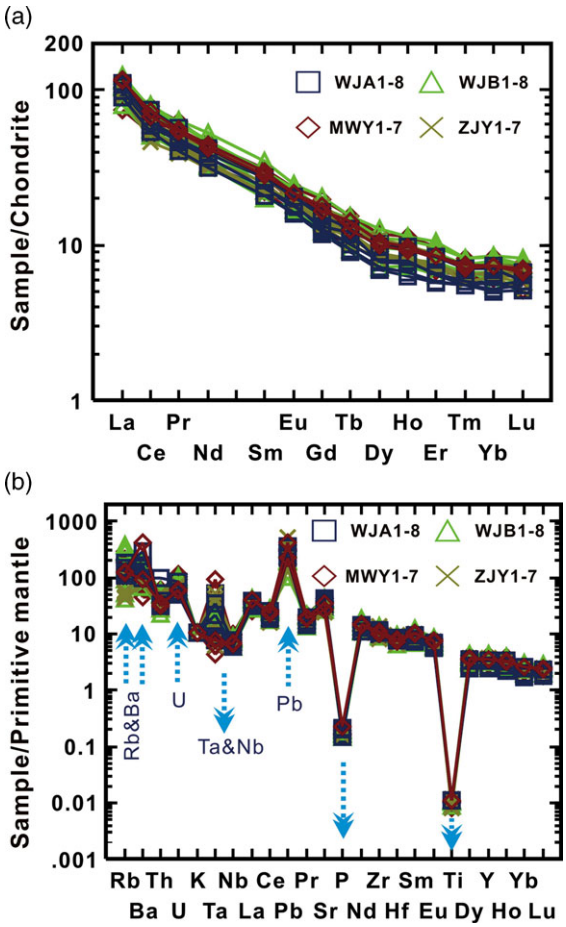

Fig. 8. (Colour online) (a) Chondrite-normalized REE and (b) primitive-mantle-normalized multi-element variation diagrams for the mafic dykes studied. Concentrations are normalized to chondrite composition of Sun and McDonough (1989).

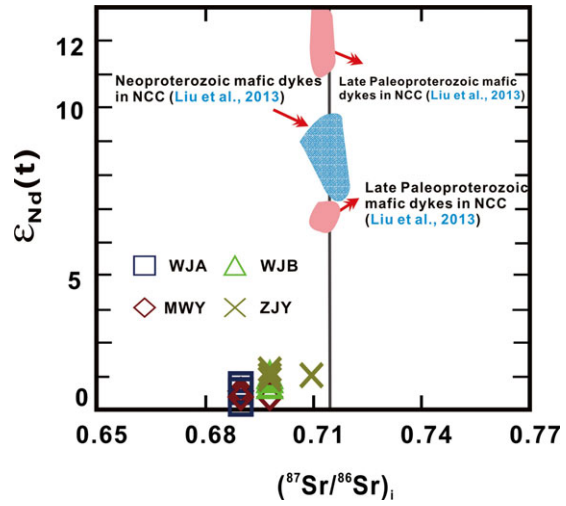

Fig. 9. (Colour online) Variations in initial $^{87}Sr/^{86}Sr$ vs $\epsilon_{Nd}(t)$ values for the mafic dykes studied. The field delineates the composition of Proterozoic mafic dykes within the NCC (Liu *et al.* 2013*b*). The mafic dykes analysed during this study plot within the isotope-depleted mantle source field.

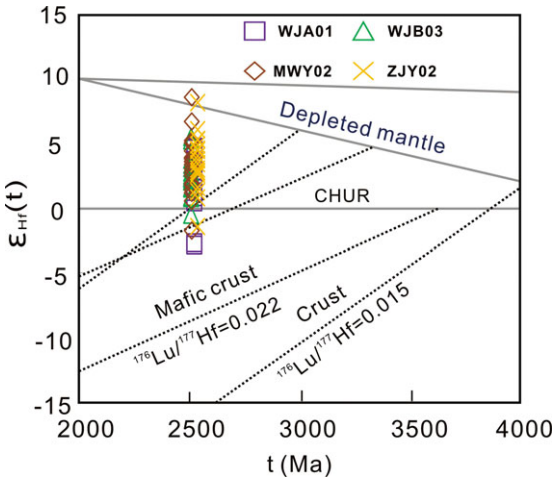

Fig. 10. (Colour online) Plots of zircon ages vs $\epsilon_{Hf}(t)$ values for the mafic dykes studied.

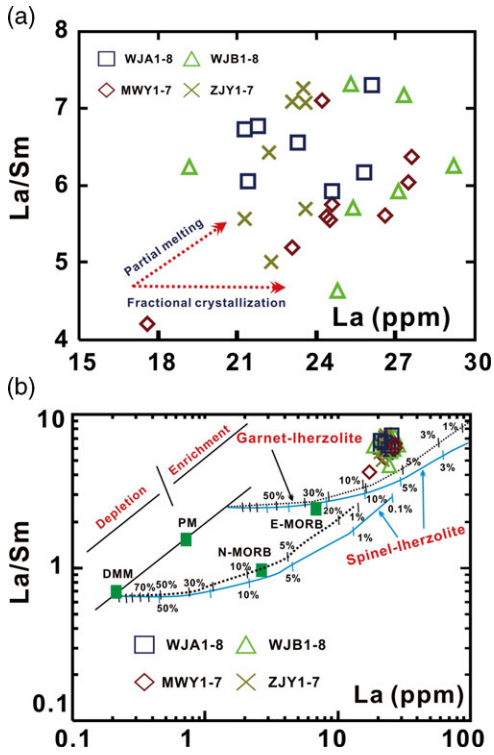

Fig. 11. (Colour online) Variations in La vs La/Sm and Sm vs Sm/Yb of the mafic dykes studied.

6. Conclusions

1. Zircon LA-ICP-MS U–Pb dating indicates that the mafic dykes from Shandong province in the northeastern NCC formed between 2509 ± 6.1 and 2537 ± 6.2 Ma, indicative of a Neoarchaean mafic magmatic event.
2. These mafic dykes are alkaline and shoshonitic. They are characterized by high light rare earth element (LREE) concentrations ($(La/Yb)_N$ between 7.17 and 8.55), positive Eu (Eu/Eu* between 1.12 and 1.27), Ba, K, Pb and Sr anomalies,

https://doi.org/10.1017/S0016756822000784 Published online by Cambridge University Press

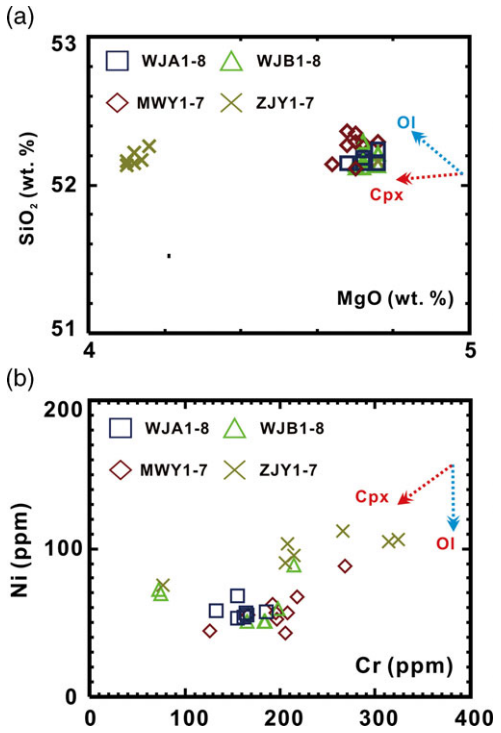

Fig. 12. (Colour online) The correlative plots MgO vs SiO_2 (a) and Cr vs Ni (b) for the mafic dykes studied.

and negative Nb, P, Ta and Ti anomalies. The dykes have low initial $(^{87}Sr/^{86}Sr)_i$ values of ~0.6969, high $\epsilon_{Nd}(t)$ (0.2–0.8) and $\epsilon_{Hf}(t)$ values (0.5–8.6, except for a few samples). They were likely derived from melting (10–20 %) of an isotope-depleted garnet–lherzolite mantle that was hybridized by foundered lower crustal material.

3. The mantle-derived parent magma of the basic vein in the study area was affected by crustal pollution to a certain extent during the magma ascent.

Acknowledgements. This research was supported by the Most Special Fund of the State Key Laboratory of Continental Dynamics, Northwest University, the National Natural Science Foundation of China (41373028, 41573022) and Shaanxi Provincial Natural Science Basic Research Program Project (2023-JC-ZD-16). The authors thank Honglin Yuan and Liang Qi for assistance during zircon Hf isotope, Sr–Nd isotope and trace element analyses, and the zircon U–Pb dating.

References

Andersen T (2002) Correction of common lead in U-Pb analyses that do not report ^{204}Pb. *Chemical Geology* **192**, 59–79.

Anderson DA (2006) Speculations on the nature and cause of mantle heterogeneity. *Tectonophysics* **146**, 7–22.

Arndt NT and Goldstein SL (1989) An open boundary between lower continental crust and mantle: its role in crust formation and crustal recycling. *Tectonophysics* **161**, 201–12.

Budnick RL (1995) Making continental crust. *Nature* **378**, 571–8.

Chen L, Diwu CR and Wang HL (2009) Crust format ion in the Ordos block: constraints from detrital zircons from Ordovician and Permian sandstones. In *Abstract with Program of International Discussion Meeting on Continental Geology and Tectonics*, p. 17. Xi'an: Northwest University Press.

Chen XD and Shi LB (1983) Primary research on the diabase dyke swarms in Wutai-Taihang area. *Chinese Science Bulletin* **16**, 1002–5.

Chen XD and Shi LB (1994) Basic dyke swarms in extensional structures. In *Extensional Structures* (ed. XL Qian), pp. 71–4. Beijing: Geological Publishing House.

Chen XD, Shi LB and Jia SF (1992) Proterozoic basic dyke swarms in North China. *Seismology and Geology* **14**, 351–7 (in Chinese with English abstract).

Chung SL, Wang KL and Crawford AJ (2001) High Mg potassic rocks from Taiwan: implications for the genesis of orogenic potassic lavas. *Lithos* **59**, 153–70.

Dan W, Li XH, Guo JH, Liu Y and Wang XG (2012) Paleoproterozoic evolution of the eastern Alxa Block, westernmost North China: evidence from in situ zircon U-Pb dating and Hf-O isotopes. *Gondwana Research* **21**, 838–64.

Dan W, Li XH, Wang Q, Wang XC and Liu Y (2014) Neoproterozoic S-type granites in the Alxa block, westernmost North China and tectonic implications: in situ zircon U-Pb-Hf-O isotopic and geochemical constraints. *American Journal of Science* **314**, 110–53.

Deng J, Wang Q and Li G (2017) Tectonic evolution, superimposed orogeny, and composite metallogenic system in China. *Gondwana Research* **50**, 216–66.

DePaolo DJ (1981) Trace element and isotopic effects of combined wallrock assimilation and fractional crystallization. *Earth and Planetary Science Letters* **53**, 189–202.

Diwu CR, Sun Y, Yuan HL, Wang HL, Zhong XP and Liu XM (2008) Detrital zircon U-Pb chronology: Hf isotopic and geological significance of Songshan quartzites from Dengfeng, Henan. *Chinese Science Bulletin* **53**, 1923–34 (in Chinese).

Elkins-Tanton LT (2005) Continental magmatism caused by lithospheric delamination. In *Plates, Plumes, and Paradigms* (eds GR Foulger, JH Natland, D Presnall and DL Anderson), pp. 449–62. Boulder, Colorado: Geological Society of America, Special Paper 388.

Feng GY, Liu S, Zhong H, Feng CX, Coulson IM, Qi YQ, Yang YH and Yang CG (2012) U-Pb zircon geochronology, geochemical, and Sr-Nd isotopic constraints on the age and origin of basaltic porphyries from western Liaoning province, China. *International Geology Review* **54**, 1052–1070.

Gao LZ, Zhao T, Wang YS, Zhao X, Ma YS and Yang SZ (2005) Zircon U-Pb SHRIMP ages of Precambrian basement in Yuntai Mountains, Jiaozuo, Henan. *Geological Bulletin of China* **24**, 1089–93 (in Chinese with English abstract).

Gao S and Jin ZM (1997) Delamination and its geodynamical significance for the crust-mantle evolution. *Geological Science and Technology Information* **16**, 1–9 (in Chinese with English abstract).

Gao S, Luo TC, Zhang BR, Zhang HF, Han YW, Zhao ZD and Hu YK (1998a) Chemical composition of the continental crust as revealed by studies in East China. *Geochimica et Cosmochimica Acta* **62**, 1959–75.

Gao S, Rudnick RL, Xu WL, Yuan HL, Liu YS, Walker RJ, Puchtel I, Liu XM, Huang H, Wang XR and Yang J (2008) Recycling deep cratonic lithosphere and generation of intraplate magmatism in the North China Craton. *Earth and Planetary Science Letters* **270**, 41–53.

Gao S, Rudnick RL, Yuan HL, Liu XM, Liu YS, Xu WL, Ling WL, Ayers J, Wang XC and Wang QH (2004) Recycling lower continental crust in the north China craton. *Nature* **432**, 892–7.

Gao S, Zhang BR, Jin ZM, Kern H, Luo TC and Zhao ZD (1998b) How mafic is the lower continental crust? *Earth and Planetary Science Letters* **106**, 101–17.

Gao S, Zhang BR, Luo TC, Li ZJ and Gao CL (1992) Chemical composition of the continental crust in the Qinling Belt and its adjacent North China and Yangtze Cratons. *Geochimica et Cosmochimica Acta* **36**, 3933–50.

Geng YS, Yang CH, Wang XR, Ren LD, Du LL and Zhou XW (2007) Ages of crystallized basement in western margin of the Yangtze platform. *Geological Journal China Universities* **34**, 251–61 (in Chinese with English abstract).

Goldfarb R and Santosh M (2014) The dilemma of the Jiaodong gold deposits: are they unique? *Geoscience Frontiers* **5**, 139–53.

Griffin DR (1992) *Animal Minds*. Chicago: University of Chicago Press.

Griffin WL, Pearson NI, Belousova EA and Saeed A (2006) Comment: Hf-isotope heterogeneity in zircon 91500. *Chemical Geology* **233**, 358–63.

Griffin WL, Zhang AD, O'Reilly SY and Ryan CG (1998) Evolution of the lithosphere beneath the Sino-Korean Craton. In *Mantle Dynamics and Plate Interactions in East Asia* (eds MFJ Flower, SL Chung, CH Lo and

https://doi.org/10.1017/S0016756822000784 Published online by Cambridge University Press

TY Lee), pp. 107–26. Washington, DC: American Geophysical Union, Geodynamics Series 27.

Guo F, Fan WM, Wang YJ and Li CW (2004) When did the Emeishan mantle plume activity start? Geochronological and geochemical evidence from ultramafic-mafic dykes in southwestern China. *International Geology Review* **46**, 226–34.

Guo F, Guo JT, Wang YC, Fan WM, Li CW, Zhao L, Li HX and Li JY (2013) Formation of mafic magmas through lower crustal AFC processes: an example from the Jinan gabbroic intrusion in the North China Block. *Lithos* **179**, 157–74.

Guo JH, Sun M, Chen FK and Zhai MG (2005) Sm-Nd and SHRIMP U-Pb zircon geochronology of high-pressure granulites in the Sanggan area, North China Craton: timing of Palaeoproterozoic continental collision. *Journal of Asian Earth Sciences* **24**, 629–42.

Herzberg C, Asimow PD, Arndt N, Niu Y, Lesher CM, Fitton JG, Cheadle MJ and Saunders AD (2007) Temperatures in ambient mantle and plumes: constraints from basalts, picrites, and komatiites. *Geochemistry, Geophysics, Geosystems* **8**, 1525–2027.

Hirajima T, Ishiwatari A, Cong B, Zhang R, Banno S and Nozaka T (1990) Coesite from Mengzhong eclogite at Donghai county, northern Jiangsu province, China. *Mineralogical Magazine* **54**, 579–83.

Hou GT (2012) *Mafic Dyke Swarms of North China*. Science Press, 177 pp. (in Chinese with English abstract).

Hou GT, Li JH, Lin AW and Qian XL (2004) New comment on the early Precambrian tectono-magmatic subdivision and evolution in the western Shandong Block. *Geological Journal of China Universities* **10**, 239–49 (in Chinese with English abstract).

Hou GT, Liu YL and Li JH (2006) Evidence for 1.8 Ga extension of the Eastern Block of the North China Craton from SHRIMP U-Pb dating of mafic dyke swarms in Shandong Province. *Journal of Asian Earth Sciences* **27**, 392–401.

Huang X, Bi Z and DePaolo DJ (1986) Sm-Nd isotope study of Early Archean rocks, Qian an, Hebei Province, China. *Geochimica et Cosmochimica Acta* **50**, 625–31.

Jahn BM (1988) Archean crustal evolution in China: the Taishan Complex, and evidence for juvenile crustal addition from long-term depleted mantle. *Precambrian Research* **38**, 381–403.

Jahn BM and Bai YL (1983) Early Archean (3.5 Ga) metabasic rocks from the Tsao Zhuang Group, E Hebei, China: Sm-Nd, common Pb and Rb-Sr isotopic ages. In *Symposium "Precambrian Crustal Evolution"*, Beijing: Chinese Academy of Geological Sciences.

Jahn BM, Wu FY, Lo CH and Tsai CH (1999) Crust mantle interaction induced by deep subduction of the continental crust: geochemical and Sr-Nd isotopic evidence from post-collisional mafic-ultramafic intrusions of the northern Dabie complex, central China. *Chemical Geology* **157**, 119–46.

Ju W, Hou GT and Zhang B (2014) Insights into the damage zones in fault-bend folds from geomechanical models and field data. *Tectonophysics* **610**, 182–94.

Jull M and Kelemen PB (2001) On the conditions for lower crustal convective instability. *Journal of Geophysical Research* **106**, 423–46.

Kato T, Nami A and Zhai M (1997) Ultrahigh-pressure marble and eclogite in the Su-Lu ultrahigh-pressure terrane, eastern China. *Journal of Metamorphic Geology* **15**, 169–82.

Kay RW and Kay SM (1991) Creation and destruction of lower continental crust. *Geologists Rundschau* **80**, 259–78.

Kogiso T, Hirschmann MM and Frost DJ (2003) High-pressure partial melting of garnet pyroxenite: possible mafic lithologies in the source of ocean island basalts. *Earth and Planetary Science Letters* **216**, 603–17.

Le Maitre RW (2002) *Igneous Rocks: A Classification and Glossary of Terms*, 2nd edn. Cambridge: Cambridge University Press, 236 pp.

Levander A, Niu F, Lee CTA and Cheng X (2006) Imaging the continental lithosphere. *Tectonophysics* **416**, 167–85.

Li JH, He WY and Qian XL (1997) The genetic mechanism of mafic dyke swarm and the reconstruction of ancient plate. *Geological Journal of China Universities* **3**, 2–8 (in Chinese with English abstract).

Li SR and Santosh M (2017) Geodynamics of heterogeneous gold mineralization in the North China Craton and its relationship to lithospheric destruction. *Gondwana Research* **50**, 267–92.

Li SZ and Zhao GC (2007) SHRIMP U-Pb zircon geochronology of the Liaoji granitoids: constraints on the evolution of the Paleoproterozoic Jiao-Liao-Ji belt in the Eastern Block of the North China Craton. *Precambrian Research* **158**, 1–16.

Li SZ, Zhao GC, Santosh M, Liu X, Lai LM, Suo YH, Song MC and Wang PC (2012) Paleoproterozoic structural evolution of the southern segment of the Jiao-Liao-Ji Belt, North China Craton. *Precambrian Research* **200–203**, 59–73.

Li SZ, Zhao GC, Sun M, Han ZZ, Zhao GT and Hao DF (2006) Are the South and North Liaohe Groups of the North China Craton different exotic terranes? Nd isotope constraints. *Gondwana Research* **9**, 198–208.

Li TS, Zhai MG, Peng P, Chen L and Guo J (2010) 2.5 billion year old coeval ultramafic-mafic and syenitic dykes in Eastern Hebei: implications for cratonization of the North China Craton. *Precambrian Research* **180**, 143–55.

Li XP, Yang ZY, Zhao GC, Grapes R and Guo JH (2011) Geochronology of khondalite-series rocks of the Jining Complex: confirmation of depositional age and tectonometamorphic evolution of the North China Craton. *International Geology Review* **53**, 1194–211.

Li Y (2014) *The comparative study on the mafic dykes between 1.6 Ga and 1.8 Ga from western Shandong province, North China Craton*. Master's thesis, University of Chinese Academy of Sciences, Beijing, China.

Liu DY (1991) Discovery of old continental crust in China. *Geology in China* **5**, 30 (in Chinese with English abstract).

Liu DY, Nutman AP, Williams JS, Compston W, Wu JS and Shen QH (1994) The remnants of 3800 Ma crust in Sino-Korean Craton: the evidence from ion microprobe U-Pb dating of zircons. *Acta Geoscientica Sinica* **1–2**, 1–13 (in Chinese with English abstract).

Liu DY, Nutman APW, Compston W, Wu JS and Shen QH (1992) Remnants of 3800 Ma crust in the Chinese part of the Sino-Korean Craton. *Geology* **20**, 339–42.

Liu S, Feng Cx, Jahn BM, Hu RZ, Zhai MG and Lai SC (2014) Zircon U-Pb age, geochemical, and Sr-Nd isotopic constraints on the origin of late Carboniferous mafic dykes of the north China Craton, Shanxi province, China. *Acta Petrologica Sinica* **30**, 1707–1717.

Liu S, Feng CX, Feng GY, Xu MJ, Coulson IM, Guo XL, Guo Z, Peng H and Feng Q (2017) Timing, mantle source and origin of mafic dykes within the gravity anomaly belt of the Taihang-Da Hinggan gravity lineament, central North China Craton. *Journal of Geodynamics* **109**, 41–58.

Liu S, Feng CX, Hu RZ, Zhai MG, Gao S, Lai SC, Yan J, Coulson IM and Zou HB (2015) Zircon U-Pb geochronological, geochemical, and Sr-Nd isotope data for early Cretaceous mafic dykes in the Tancehng-Lujiang Fault area of the Shandong province, China: Constraints on the timing of magmatism and magma genesis. *Journal of Asian Earth Sciences* **99**, 247–260.

Liu S, Feng CX, Jahn BM, Hu RZ, Gao S, Coulson IM, Feng GY, Lai SC, Yang CG and Yang YH (2013a) Zircon U-Pb age, geochemical, and Sr-Nd-Hf isotopic constraints on the origin of mafic dykes in the Shaanxi Province, North China Craton, China. *Lithos* **175-176**, 244–254.

Liu S, Feng CX, Jahn BM, Hu RZ, Gao S, Coulson IM, Feng GY, Lai SC, Yang YH and Tang L (2013c) Geochemical, Sr-Nd-Pb isotope, and zircon U-Pb geochronological constraints on the origin of Early Permian mafic dykes, northern North China Craton. *International Geology Review* **55**, 1626–1640.

Liu S, Feng CX, Jahn BM, Hu RZ, Gao S, Feng GY, Lai SC, Yang YH, Qi YQ and Coulson IM (2013b) Geochemical, Sr-Nd isotopic, and zircon U-Pb geochronological constraints on the petrogenesis of Late Paleoproterozoic mafic dykes within the northern North China Craton, Shanxi Province, China. *Precambrian Research* **206**, 182–92.

Liu S, Feng CX, Santosh M, Feng GY, Coulson IM, Xu MJ, Guo Z, Guo XL, Peng H and Feng Q (2018) Integrated elemental Sr-Nd-Pb-Hf isotopic studies of Mesozoic mafic dykes from the eastern North China Craton: implications for the dramatic transformation of Mlithospheric mantle. *Journal of Geodynamics* **114**, 19–40.

Liu S, Feng CX, Zhai MG, Hu RZ and Yan J (2016) Zircon U-Pb age, geochemical, and Sr-Nd-Hf isotopic constraints on the origin of early Cretaceous mafic dykes from western Shandong province, eastern North China Craton. *Acta Petrologica Sinica* **32**, 629–645.

Liu S, Hu RZ, Gao S, Feng CX, Coulson IM, Feng GY, Qi YQ, Yang YH, Yang CG and Tang L (2012a) U-Pb zircon age, geochemical and Sr-Nd isotopic data as constraints on the petrogenesis and emplacement time of the

https://doi.org/10.1017/S0016756822000784 Published online by Cambridge University Press

Precambrian mafic dyke swarms in the North China Craton (NCC). *Lithos* **140-141**, 38-52.

Liu S, Hu RZ, Gao S, Feng CX, Feng GY, Coulson IM, Li C, Wang T and Qi YQ (2010c) Zircon U-Pb age and Sr-Nd-Hf isotope geochemistry of Permian granodiorite and associated gabbro in the Songliao Block, NE China and implications for growth of juvenile crust. *Lithos* **114**, 423–436.

Liu S, Hu RZ, Gao S, Feng CX, Qi L, Zhong H, Xiao TF, Qi YQ, Wang T and Coulson IM (2008b) Zircon U-Pb geochronology and major, trace elemental and Sr-Nd-Pb isotopic geochemistry of mafic dykes in western Shandong Province, east China: constraints on their petrogenesis and geodynamic significance. *Chemical Geology* **255**, 329–45.

Liu S, Hu RZ, Gao S, Feng CX, Qi YQ, Wang T, Feng GY and Coulson IM (2008a) U-Pb zircon age, geochemical and Sr-Nd-Pb-Hf isotopic constraints on age and origin of alkaline intrusions and associated mafic dykes from Sulu orogenic belt, Eastern China. *Lithos* **106**, 365–79.

Liu S, Hu RZ, Gao S, Feng CX and Tang L (2012b) Geochemical and isotopic constraints on the age and origin of mafic dikes from Eastern Shandong province, Eastern North China Craton, China. *International Geology Review* **54**, 1389–1400.

Liu S, Hu RZ, Gao S, Feng CX, Yu BB, Feng GY, Qi YQ, Wang T and Coulson IM (2009) Petrogenesis of Late Mesozoic mafic dykes in the Jiaodong Peninsula, eastern North China Craton and implications for the foundering of lower crust. *Lithos* **113**, 621–39.

Liu S, Hu RZ, Zhao JH and Feng CX (2004) K-Ar ages of Mesozoic mafic dyke rocks and crustal extension in Shandong Province, eastern China. *Acta Geologica Sinica* **78**, 1207–1213.

Liu S, Hu RZ, Zhao JH, Feng CX, Zhong H, Cao JJ and Shi DN (2005) Geochemical characteristics and petrogenetic investigation of the Late Mesozoic lamprophyres of Jiaobei, Shandong province. *Acta Petrologica Sinica* **21**, 947–58 (in Chinese with English abstract).

Liu S, Hu RZ, Gao S, Feng CX, Zhong H, Qi YQ, Wang T, Feng GY and Yang YH (2011) U-Pb zircon age along with geochemical and Sr-Nd-Pb isotopic constraints on the dating and origin of intrusive complexes from the Sulu orogenic belt, Eastern China. *International Geology Review* **53**, 61–83.

Liu S, Su WC, Hu RZ, Feng XC, Gao S, Coulosn IM, Wang T, Feng GY, Tao Y and Xia Y (2010b) Geochronological and geochemical constraints on the petrogenesis of alkaline ultramafic dykes from southwest Guizhou Province, SW China. *Lithos* **114**, 253–264.

Liu S, Zou HB, Hu RZ, Zhao JH and Feng CX (2006) Mesozoic mafic dikes from the Shandong Peninsula, North China Craton: Petrogenesis and tectonic implications. *Geochemical Journal* **40**, 181–195.

Liu YS, Hu ZC, Zong KQ, Gao CG, Gao S, Xu J and Chen HH (2010a) Reappraisement and refinement of zircon U-Pb isotope and trace element analyses by LA-ICP-MS. *Chinese Science Bulletin* **55**, 1535–46.

Ludwig KR (2003) User's manual for Isoplot/Ex version 3.00, a geochronological toolkit for Microsoft Excel. Berkeley Geochronology Center Special Publications 4, 72.

Lugmair GW and Harti K (1978) Lunar initial $^{143}Nd/^{144}Nd$: differential evolution of the lunar crust and mantle. *Earth and Planetary Science Letters* **39**, 349–57.

Luo Y, Sun M, Zhao GC, Ayers JC, Li SZ, Xia XP and Zhang JH (2008) A comparison of U-Pb and Hf isotopic compositions of detrital zircons from the North and South Liaohe Group: constraints on the evolution of the Jiao-Liao-Ji Belt, North China Craton. *Precambrian Research* **16**, 279–306.

Luo ZH, Wei Y, Xin HT, Zhang HM, Ke S and Li WT (2006) Petrogenes of the post-orogenic dyke complex-constraints to thioshpere deamination. *Acta Petrologica Sinica* **22**, 1672–84 (in Chinese with English abstract).

Lustrino M (2005) How the delamination and detachment of lower crust can influence basaltic magmatism. *Earth-Science Reviews* **72**, 21–38.

Menzies MA and Kyle PR (1972) Continental volcanism: a crust-mantle probe. In *Continental Mantle* (ed MA Menzies), pp. 157–77. Oxford: Oxford University Press.

Middlemost EAK (1994) Naming materials in the magma/igneous rock system. *Earth-Science Reviews* **74**, 193–227.

Muller D, Franz L, Herzig PM and Hunt S (2001) Potassic igneous rocks from the vicinity of epithermal gold mineralization. Lihir Island, Papua New Guinea. *Lithos* **57**, 163–85.

Nelson DR (1992) Isotopic characteristics of potassic rocks: evidence for the involvement of subducted sediments in the magma genesis. *Lithos* **28**, 403–20.

Niu YL, Wilson M, Humphreys ER and O'Hara MJ (2011) The origin of intraplate Ocean Island Basalts (OIB): The lid effect and its geodynamic implications. *Journal of Petrology* **52**, 1443–1468.

O'Reilly SY, Griffin WL, Poudjom Djomani YH and Morgan P (2001) Are lithospheres forever? Tracking changes in sub-continental lithospheric mantle through time. *GSA Today* **11**, 4–10.

Peng P (2010) *Reconstruction and interpretation of giant mafic dyke swarms: a case study of 1.78 Ga magmatism in the North China Craton*. In *The Evolving Continents: Understanding Processes of Continental Growth* (ed. TM Kusky), pp. 163–78. Geological Society of London, Special Publication no. 338.

Peng P, Bleeker W, Ernst RE, Söderlund U and McNicoll V (2011a) U-Pb baddeleyite ages, distribution and geochemistry of 925 Ma mafic dykes and 900 Ma sills in the North China craton: evidence for a Neoproterozoic mantle plume. *Lithos* **127**, 210–21.

Peng P, Guo JH, Zhai MG and Bleeker W (2010) Paleoproterozoic gabbronoritic and granitic magmatism in the northern margin of the North China Craton: evidence of crust–mantle interaction. *Precambrian Research* **183**, 635–59.

Peng P, Zhai MG, Guo JH, Kusky T and Zhao TP (2007) Nature of mantle source contributions and crystal differentiation in the petrogenesis of the 1.78 Ga mafic dykes in the central North China craton. *Gondwana Research* **12**, 29–46.

Peng P, Zhai MG, Li QL, Wu FY, Hou QL, Li Z, Li TS and Zhang YB (2011b) Neoproterozoic (900 Ma) Sariwon sills in North Korea: geochronology, geochemistry and implications for the evolution of the south-eastern margin of the North China Craton. *Gondwana Research* **20**, 243–54.

Peng P, Zhai MG, Li Z, Wu FY and Hou QL (2008) Neoproterozoic (~820 Ma) mafic dyke swarms in the North China craton: implication for a conjoint to the Rodinia supercontinent? *Abstracts, 13th Gondwana Conference,* September 15–22, 160–1, Elsevier, Netherlands, Kerala, India.

Peng P, Zhai MG, Zhang HF and Guo JH (2005) Geochronological constraints on the Palaeoproterozoic evolution of the North China Craton: SHRIMP zircon ages of different types of mafic dykes. *International Geology Review* **47**, 492–508.

Potts PJ and Kane JS (2005) International association of geoanalysts certificate of analysis: certified reference material OU-6 (Penrhyn slate). *Geostandards and Geoanalytical Research* **29**, 233–6.

Qi L, Hu J and Grégoire DC (2000) Determination of trace elements in granites by inductively coupled plasma mass spectrometry. *Talanta* **51**, 507–13.

Qi YQ, Hu RZ, Liu S, Coulson IM, Qi HW, Tian JJ, Feng CX and Wang T (2012) Geochemical and Sr-Nd-Pb isotopic compositions of Mesjozoic mafic dykes from the Gan-Hang tectonic belt, south China: petrogenesis and geodynamic significance. *International Geology Review* **54**, 920–939.

Rapp RP, Shimizu N and Norman MD (2003) Growth of early continental crust by partial melting of eclogite. *Nature* **425**, 605–9.

Rapp RP, Shimizu N, Norman MD and Applegate GS (1999) Reaction between slab-derived melts and peridotite in the mantle wedge: experimental constraints at 3.8 GPa. *Chemical Geology* **160**, 335–56.

Regional Geology of Shandong Province (1995) Beijing: Geological Publishing House, 1–533 pp.

Rogers NW and Setterfle TN (1994) Potassium and incompatible element enrichment in shoshonitic lavas from the Tavua volcano, Fiji. *Chemical Geology* **118**, 43–62.

Rudnick RL and Fountain DM (1995) Nature and composition of the continental crust: a lower crustal perspective. *Reviews of Geophysics* **33**, 267–309.

Santosh M (2010) Assembling North China Craton within the Columbia supercontinent: the role of double-sided subduction. *Precambrian Research* **178**, 149–67.

Shao JA and Zhang LQ (2002) Mesozoic dyke swarms in the north of North China. *Acta Petrologica Sinica* **18**, 312–8 (in Chinese with English abstract).

Shen QH, Geng YS, Song B and Wan YS (2005) New informations of Earth surface and deep crust from the North China Block, Yangtze Block and Qinling-Dabie orogenic belt. *Acta Geologica Sinica* **79**, 616–27 (in Chinese with English abstract).

https://doi.org/10.1017/S0016756822000784 Published online by Cambridge University Press

Sobolev AV, Hofmann AW, Kuzmin DV, Yaxley GM, Arndt NT, Chung SL, Danyushevsky LV, Elliott T, Frey FA, Garcia MO, Gurenko AA, Kamenetsky VS, Kerr AC, Krivolutskaya NA, Matvienkov VV, Nikogosian IK, Rocholl A, Sigurdsson IA, Sushchevskaya NM and Teklay M (2007) The amount of recycled crust in sources of mantle-derived melts. *Science* **316**, 412–7.

Sobolev AV, Hofmann AW, Sobolev SV and Nikogosian IK (2005) An olivine-free mantle source of Hawaiian shield basalts. *Nature* **434**, 590–7.

Song B, Allen PN, Liu DY and Wu JS (1996) 3800 to 2500 Ma crustal evolution the Anshan area of Liaoning Province, northeastern China. *Precambrian Research* **78**, 79–94.

Steiger RH and Jäger E (1977) Subcommission on geochronology; convention on the use of decay constants in geochronology and cosmochronology. *Earth and Planetary Science Letters* **36**, 359–362.

Sun SS and McDonough WF (1989) Chemical and isotopic systematics of oceanic basalts; implications for mantle composition and processes. In *Magmatism in the Ocean Basins* (eds AD Saunders and MJ Norry) pp. 313–45. Geological Society of London, Special Publication no. 42.

Tam PY, Zhao GC, Liu FL, Zhou XW, Sun M and Li SZ (2011) SHRIMP U-Pb zircon ages of high-pressure mafic and pelitic granulites and associated rocks in the Jiaobei massif: constraints on the metamorphic ages of the Paleoproterozoic Jiao-Liao-Ji Belt in the North China Craton. *Gondwana Research* **19**, 150–62.

Tam PY, Zhao GC, Sun M, Li SZ, Iizukac Y, Ma SK, Yin CQ, He YH and Wu ML (2012a) Metamorphic P-T path and tectonic implications of medium-pressure politic granulites from the Jiaobei massif in the Jiao-Liao-Ji Belt, North China Craton. *Precambrian Research* **220–221**, 177–91.

Tam PY, Zhao GC, Sun M, Li SZ, Wu ML and Yin CQ (2012b) Petrology and metamorphic P-T path of high-pressure mafic granulites from the Jiaobei massif in the Jiao-Liao-Ji Belt, NCC. *Lithos* **155**, 94–109.

Tam PY, Zhao GC, Zhou XW, Sun M, Li SZ, Yin CQ, Wu ML and He YH (2012c) Metamorphic P–T path and implications of high-pressure pelitic granulites from the Jiaobei massif in the Jiao-Liao-Ji Belt, NCC. *Gondwana Research* **22**, 104–17.

Tang L and Santosh M (2017) Neoarchean granite-greenstone belts and related ore mineralization in the North China Craton: an overview. *Geoscience Frontiers* **3**, 751–68.

Taylor SR and McLennan SM (1985) *The Continental Crust: Its Composition and Evolution*. Oxford: Blackwell.

Thompson M, Potts PJ, Kane JS and Wilson S (2000) An international proficiency test for analytical geochemistry laboratories: report on round 5 (August 1999). *Geostandards and Geoanalytical Research* **24**, 1–28.

Wan YS, Liu DY and Song B (2005) Geochemical and Nd isotopic composition of 3.8 Ga meta-quartz dioritic and trondhjemitic rocks from the Archean area and their geological significance. *Journal of Asian Earth Science* **24**, 563–75.

Wang F, Li XP, Chu H and Zhao GC (2011) Petrology and metamorphism of khondalites from Jining Complex in the North China Craton. *International Geology Review* **53**, 212–29.

Wang HL, Chen L, Sun Y, Liu XM, Xu XY, Chen JL, Zhang H and Diwu CR (2007) Discovery of ca. 4.1 Ga trapped zircon. *Chinese Science Bulletin* **52**, 1685–93 (in Chinese).

Wang LQ, Qiu YM, McNaughton NL, Groves DI, Luo ZK, Huang JZ, Miao LC and Liu YK (1998) Constraints on crustal evolution and gold metallogeny in the northwestern Jiaodong, China, from SHRIMP U-Pb zircon studies of granitoids. *Ore Geology Review* **13**, 275–91.

Wang SJ (1990) The Precambrian rocks in western Shandong province, China. *Shandong Geology* **6**, 59–80 (in Chinese with English abstract).

Wang SJ (1991) Stage and phase division and basic features of Precambrian intrusive rocks in the western Shandong Province. *Regional Geology in China* **4**, 298–307 (in Chinese with English abstract).

Wang SJ (1993) Early Precambrian geotectonic in the western Shandong. *Regional Geology in China* **3**, 216–22 (in Chinese with English abstract).

Wang XS, Zhuang YX and Xu HF (1999) The significance of terminal Archean ductile shearing in continental crustal evolution of the Taishan Mountain region. *Regional Geology in China* **18**, 168–74 (in Chinese with English abstract).

Wang YM, Gao YS, Han HM and Wang XH (2003) *Practical Handbook of Reference Materials for Geoanalysis*. Beijing: Geological Publishing House (in Chinese).

Weaver BI (1991) The origin of ocean island end-member compositions: trace element and isotopic constraints. *Earth and Planetary Science Letters* **104**, 381–97.

Wedepohl KH (1991) Chemical composition and fractionation of the continental crust. *Geologische Rundschau* **80**, 207–23.

Wilde SA, Zhao GC and Sun M (2002) Development of the North China craton during the Late Archaean and its final amalgamation at 1.8 Ga: some speculation on its position within a global Palaeoproterozoic Supercontinent. *Gondwana Research* **5**, 85–94.

Wu FY, Walker RJ, Yang YH, Yuan HL and Yang HH (2006) The chemical-temporal evolution of lithospheric mantle underlying the North China Craton. *Geochimica et Cosmochimica Acta* **70**, 5013–34.

Wu FY, Xu YG, Gao S and Zheng JP (2008) Lithospheric thinning and destruction of the North China Craton. *Acta Petrologica Sinica* **24**, 1145–74 (in Chinese with English abstract).

Wu JS, Geng YS, Shen QH, Wang YS, Liu DY and Song B (1998) *Archean Geological Nature and Tectonic Evolution of Sino-Korean Continent*. Beijing: Geological Publishing House, —212 pp. (in Chinese with English abstract).

Xia XP, Sun M, Zhao GC, Wu FY, Xu P and Zhang JS (2008) Paleoproterozoic crustal growth events in the Western Block of the North China Craton: evidence from detrital zircon Hf and whole rock Sr-Nd isotopes of the khondalites in the Jining Complex. *American Journal of Science* **308**, 304–27.

Xu YG (2001) Thermo-tectonic destruction of the Archean lithospheric keel beneath the Sino-Korean Craton in China: evidence, timing and mechanism. *Physics and Chemistry of the Earth* **26**, 747–57.

Yang JH, Wu FY, Chung SL, Wilde SA and Chu MF (2006) A hybrid origin for the Qianshan A-type granite, Northeast China: geochemical and Sr-Nd-Hf isotopic evidence. *Lithos* **89**, 89–106.

Yang JH, Wu FY, Wilde SA and Liu XM (2007) Genesis of Late Triassic granites and mafic enclaves in the Liaodong Peninsula: evidence for lithospheric thinning after the collision of the North China Craton. *Bulletin of Mineralogy Petrology and Geochemistry* **Z1**, 64–66.

Yang QY and Santosh M (2017) The building of an Archean microcontinent: evidence from the North China Craton. *Gondwana Research* **50**, 3–37.

Yang QY, Santosh M, Collins AS and Teng XM (2016) Microblock amalgamation in the North China Craton: evidence from Neoarchaean magmatic suite in the western margin of the Jiaoliao Block. *Gondwana Research* **31**, 96–123.

Yaxley GM (2000) Experimental study of the phase and melting relations of homogeneous basalt plus peridotite mixtures and implications for the petrogenesis of flood basalts. *Contributions to Mineralogy and Petrology* **139**, 326–38.

Yaxley GM and Green DH (1998) Reactions between eclogite and peridotite: mantle refertilisation by subduction of oceanic crust. *Schweizerische Mineralogische und Petrographische Mitteilungen* **78**, 243–55.

Ye S, Lambert SB, Grimwood K, Roczo-Farkas S, Nimmo GR, Sloots TP, Kirkwood CD and Whiley DM (2015) Comparison of test specificities of commercial antigen-based assays and in-house PCR methods for detection of rotavirus in stool specimens. *Journal of Clinical Microbiology* **53**, 295–297.

Yin CQ, Zhao GC, Guo JH, Sun M, Zhou XW, Zhang J, Xia XP and Liu CH (2011) U-Pb and Hf isotopic study of zircons of the Helanshan Complex: constraints on the evolution of the Khondalite Belt in the Western Block of the North China Craton. *Lithos* **122**, 25–38.

Yin CQ, Zhao GC, Sun M, Xia XP, Wei CJ, Zhou XW and Leung WH (2009) LA-ICP-MS U-Pb zircon ages of the Qianlishan Complex: constraints on the evolution of the Khondalite Belt in the Western Block of the North China Craton. *Precambrian Research* **174**, 78–94.

Zhai MG (2010) Tectonic evolution and metallogenesis of North China Craton. *Mineral Deposits* **29**, 24–36 (in Chinese with English abstract).

Zhai MG and Bian AG (2000) The supercontinent assembling during Neoarchean and the cracking between Paleoproterozoic and Mesoproterozoic of the North China Craton. *Science in China* **30**, 129–37 (in Chinese with English abstract).

https://doi.org/10.1017/S0016756822000784 Published online by Cambridge University Press

Zhai MG and Peng P (2007) Paleoproterozoic events in the North China Craton. *Acta Petrologica Sinica* **23**, 1665–82 (in Chinese with English abstract).

Zhai MG and Santosh M (2011) The early Precambrian odyssey of the North China Craton: a synoptic overview. *Gondwana Research* **20**, 6–25.

Zhai MG and Santosh M (2013) Metallogeny of the North China Craton: link with secular changes in the evolving Earth. *Gondwana Research* **24**, 275–97.

Zhang CL, Liu L, Wang SJ, Liu S and Dai MN (2009) Detrital zircon provenance for the meta-sedimentary rocks from Kuanping Group: implication for Neoproterozoic reconstruction in Qinling Orogeny, central China. In *Abstract with Program of International Discussion Meeting on the Continental Geology and Tectonics* (ed. Y Yao), pp. 64–6. Xi'an: Northwest University Press.

Zhang GW, Meng QR and Lai SC (1995) Tectonics and structure of Qinling orogenic belt. *Science in China* **38**, 1379–94.

Zhang HF and Sun M (2002) Geochemistry of Mesozoic basalts and mafic dykes, southeastern north China Craton, and tectonic implications. *International Geology Review* **44**, 370–82.

Zhang HF, Sun M, Lu FX, Zhou XH, Zhou M, Liu YS and Zhang GH (2001) Geochemical significance of a garnet Iherzolite from the Dahongshan kimberlite, Yangtze Craton, southern China. *Geochemical Journal* **35**, 315–31.

Zhang HF, Sun M, Zhou XH and Ying JF (2005) Geochemical constraints on the origin of Mesozoic alkaline intrusive complexes from the North China Craton and tectonic implications. *Lithos* **81**, 297–317.

Zhang HF, Sun M, Zhou XH, Zhou MF, Fan WM and Zheng JP (2003) Secular evolution of the lithosphere beneath the eastern North China Craton: evidence from Mesozoic basalts and high-Mg andesites. *Geochimica et Cosmochimica Acta* **67**, 4373–87.

Zhang JX, Gong JH, Yu SY and Li HK (2013) Neoarchean-Paleoproterozoic multiple tectonothermal events in the western Alxa block, North China Craton and their geological implication: Evidence from zircon U-Pb ages and Hf isotopic composition. *Precambrian Research* **235**, 36–57.

Zhang Q, Li CD, Wang Y, Wang YL, Jin WJ and Han S (2005) Mesozoic high-Sr and low-Yb granitoids and low-Sr and high-Yb granitoids in eastern China: comparison and geological implications. *Acta Petrologica Sinica* **21**, 1527–37 (in Chinese with English abstract).

Zhao GC (2009) Metamorphic evolution of major tectonic units in the basement of the North China Craton; key issues and discussion. *Acta Petrologica Sinica* **25**, 1772–92.

Zhao GC (2013) *Precambrian Evolution of the North China Craton* Amsterdam: Elsevier.

Zhao GC, Sun M, Wilde SA and Li SZ (2005) Late Archaean to Palaeoproterozoic evolution of the North China Craton: key issues revisited. *Precambrian Research* **136**, 177–202.

Zhao GC, Wilde SA, Cawood PA and Sun M (2001) Archean blocks and their boundaries in the North China Craton: lithological, geochemical, structural and P-T path constraints and tectonic evolution. *Precambrian Research* **107**, 45–73.

Zhao GC and Zhai MG (2013) Lithotectonic elements of Precambrian basement in the North China Craton: review and tectonic implications. *Gondwana Research* **23**, 1207–40.

Zheng JP, Griffin WL and O'Reilly SY (2004) 3.6 Ga lower crust in central China: new evidence on the assembly of the North China Craton. *Geology* **32**, 229–32.

Zhi XC (1990) Trace element geochemistry of Tertiary continental alkalic basalt from Liuhe-Yizheng, Jiangsu province, China. *Acta Petrologica Sinica* **2**, 30–42.

Zhou XH and Armstrong RL (1982) Cenozoic volcanic rocks of eastern China-Secular and geographic trends in chemistry and strontium isotopic composition. *Earth and Planetary Science Letters* **58**, 301–329.

Zhou XW, Zhao GC, Wei CJ, Geng YS and Sun M (2008) Metamorphic evolution and Th-U-Pb zircon and monazite geochronology of high-pressure pelitic granulites in the Jiaobei massif of the North China Craton. *American Journal of Science* **308**, 328–50.

Zou HB, Zindler A, Xu XS and Qi Q (2000) Major, trace element, and Nd, Sr and Pb isotope studies of Cenozoic basalts in SE China: Mantle sources, regional variations, and tectonic significance. *Chemical Geoogy* **171**, 33–47.

https://doi.org/10.1017/S0016756822000784 Published online by Cambridge University Press